npj | vaccines

Article

Published in partnership with the Sealy Institute for Vaccine Sciences

https://doi.org/10.1038/s41541-025-01154-5

Single cell transcriptomics correlate avian coronavirus prime vaccination efficacy with antigen-presenting cell preference

Xuefeng Li[1,2,3], Yumeng Liang[2,3], Yu Zhang[2,3], Botao Fa[1,3], Zheyi Liu[1,2], Lu Cui[1,2], Miaomiao Xi[1], Shufeng Feng[1], Li Xu[2], Xiaoxiao Liu[1], Zhengtao Xiao[1] ✉, Shengwang Liu[2] ✉ & Hai Li[1,2] ✉

Biosafe and effective vaccines are urgently needed for the prevention and control of avian infectious bronchitis virus (IBV), the first coronavirus to be discovered, despite extensive vaccination for decades. However, their development has been hindered by our limited understanding of prime vaccination, which is crucial for rational vaccine design. Here, we constructed in vivo dynamic single-cell resolution blood immune landscapes of chickens immunized with live-attenuated or inactivated IBV. Bioinformatic analysis together with in vivo examination revealed that live-attenuated and inactivated vaccines reshaped lymphocytes and led to identical compositions through different mechanisms. Inactivated vaccines activate T lymphocytes through dendritic cells with subsequent T lymphocyte-dependent B lymphocyte expansion upon prime vaccination but induce pathogen-specific antibodies only after boost vaccination. Prime vaccination with a live-attenuated vaccine led to an initial preference for monocytes/macrophages as antigen-presenting cells (APCs), followed by extensive activation of the main APCs, which facilitated rapid T lymphocyte expansion and elicited satisfactory humoral immunity. Along with the disparate utilization of APCs, live-attenuated and inactivated vaccines yielded distinct TCR repertoires and triggered different B lymphocyte dynamics despite their similar final BCR repertoires. Furthermore, APC preference correlated with vaccine effectiveness rather than modality, as prime avian influenza vaccination triggered effective adaptive immune responses with the same APC preference as live-attenuated IBV did. This study comprehensively characterized avian coronavirus prime vaccination and highlighted the key role of APC preference.

Coronaviruses are the causative agents of many serious infectious diseases, such as avian infectious bronchitis (IB), transmissible gastroenteritis (TGE), porcine epidemic diarrhoea (PED), severe acute respiratory syndrome (SARS), Middle East respiratory syndrome (MERS), and coronavirus disease 2019 (COVID-19), which pose serious threats to animal and human health. As large, enveloped RNA viruses, coronaviruses are susceptible to mutation and genome recombination, leading to the constant emergence of new variants[1,2]. Avian infectious bronchitis virus (IBV), the agent that induces IB, was the first-discovered coronavirus, described in the 1930s, and is the prototypical avian coronavirus[3,4]. It is one of the major threats to the poultry industry and continuously leads to substantial economic losses worldwide[5]. Despite belonging to a different genus, IBV has many similarities in terms of structure, respiratory system pathology, and vaccination effectiveness with other coronaviruses, including human coronaviruses. Therefore, as the first identified and most extensively vaccinated-against naturally occurring coronavirus, IBV could be considered a useful model for studying the evolution, transmission, pathogenesis, and prevention of coronaviruses[6–8].

Currently, vaccination is the dominant approach for controlling IBV infections[5,9,10]. The prevention of IBV infection depends mainly on vaccination with live-attenuated vaccines, which are sufficient for protecting broilers and priming adaptive antiviral immune responses in layers and

[1]School of Basic Medical Sciences, Xi'an Jiaotong University Health Science Center, Xi'an Jiaotong University, Xi'an, PR China. [2]Division of Avian Infectious Diseases, State Key Laboratory of Animal Disease Control and Prevention, National Poultry Laboratory Animal Resource Center, Harbin Veterinary Research Institute, The Chinese Academy of Agricultural Sciences, Harbin, PR China. [3]These authors contributed equally: Xuefeng Li, Yumeng Liang, Yu Zhang, Botao Fa. ✉e-mail: zhengtao.xiao@xjtu.edu.cn; liushengwang@caas.cn; lihai@xjtu.edu.cn

breeders[11]. Inactivated vaccines are mainly administered for subsequent immune boosting in layers and breeders before the onset of egg production because of their low effectiveness in prime vaccination. However, the administration of live-attenuated vaccines promotes the emergence of new variants due to genome recombination between different viral strains[5,12]. Some of these variants are highly diverse in antigenicity, leading to low cross-protection among strains[5,9]. Therefore, despite decades of extensive vaccination, outbreaks caused by newly emerging strains are constantly occurring throughout the world. Nonlive vaccines, such as inactivated vaccines, subunit vaccines, and genetic vaccines, are biosafe, but their effectiveness is low, which is difficult to address with current strategies[13,14]. For example, at least one booster dose is currently needed to protect humans from SARS-CoV-2 infection[15].

IBV vaccines can initiate both humoral and cell-mediated immune responses[16]. The importance of humoral immunity in defending against IBV infection has been extensively proven by the more severe and longer-lasting illness and delayed clearance of the virus in bursectomized chicks and cyclophosphamide-treated chickens[17–19]. In addition, the protection of 1-day-old chicks from IBV challenge by high titre of humoral antibodies has also been demonstrated[17,20]. Nevertheless, many studies have demonstrated that cell-mediated immunity, rather than humoral immunity, is strongly correlated with complete protection against IBV challenge, suggesting that both humoral and cell-mediated immunity are important for effective protection from IBV infection[21,22]. During the initiation of antigen-specific adaptive immune responses by vaccination, the antigens delivered by vaccines are first processed by antigen-processing cells (APCs), mainly dendritic cells (DCs), macrophages, and B lymphocytes. These APCs present vaccine antigens with their MHC class II molecules and activate naïve $CD4^+$ T lymphocytes, which can specifically recognize the antigens provided by APCs. Upon activation, $CD4^+$ T lymphocytes initiate antigen-specific adaptive immune responses by activating antigen-specific B lymphocytes and $CD8^+$ cytotoxic T lymphocytes, which mediate humoral and/or cell-mediated immune responses. In humans and mice, DCs are the main APCs that can prime naïve T lymphocytes and are therefore the major APCs involved in the initiation of host adaptive immune responses upon prime vaccination[23]. However, a series of investigations revealed that the maturation and antigen presentation of DCs were effectively induced by inactivated IBV but significantly inhibited by live IBV via the induction of gga-miR21 by the non-structural proteins NSP7 and NSP16[24–26]. While, the APC responsible for the priming of naïve T lymphocytes in chickens and whether chicken DCs and macrophages exert different functions than they do in humans and mice remain to be investigated[27]. Furthermore, the productive replication of IBV in monocytes and macrophages has been observed both in vivo and in vitro[28,29]. However, its significance in chickens remains unclear. The tracheal mucosa is the portal of entry for IBV, and the tracheal mucosal immune compartment is important for tracheal protection against IBV infection. Upon extensive administration of vaccines, the tissue tropism of IBV expands from the respiratory tract to various tissues, such as the proventriculus, gizzard, kidney, bursa, ileum, jejunum, rectum, kidney, and reproductive tissues, due to viral genome recombination and mutations during the evolution of IBV under constant immune pressure[11,16]. An increasing number of studies have highlighted the increasing complexity of effective adaptive immune responses against IBV and the crucial role of systemic immune compartments. Significant efforts have been made to elucidate host immune responses against IBV infection weeks after vaccination. However, the initiation period of host adaptive immune responses against IBV upon prime vaccination, which involves complex communication among innate and adaptive immune cells, particularly the crosstalk between APCs and lymphocytes, remains largely unclear. Elucidating these complexities may be crucial for the rational design of novel biosafe and effective vaccines against IBV.

Single-cell transcriptome sequencing (scRNA-seq), which enables a comprehensive analysis of the immune system at single-cell resolution, has been widely applied in this field but has focused mainly on the effects of booster vaccination[30–33]. The dynamics of host immune responses against coronaviruses during the initiation period after prime vaccination, especially in the first two weeks after vaccination, remain largely unclear in both humans and animals. Here, detailed in vivo dynamic transcriptomic landscapes of blood immune responses elicited by live-attenuated and inactivated avian coronavirus vaccines during immune response initiation were explored and compared at single-cell resolution, together with in vivo validation analyses.

Results

Distinct dynamic PBMC landscapes after prime vaccination with live-attenuated or inactivated IBV vaccine

We first established a comparative model using 35-day-old BWEL specific-pathogen free (SPF) male chickens inoculated with live-attenuated or inactivated vaccines (six half-sibs for each group). A widely used IBV vaccine strain, H120, was used for both live-attenuated and inactivated vaccines to eliminate any influence other than the vaccine modality. As expected, the live-attenuated vaccine triggered the production of antibodies that specifically recognized the viral N protein, the most plentiful viral protein during viral replication, from 10 days post vaccination (dpv), and the antibody titer plateaued from 14 dpv (Fig. 1A). No induction of anti-N protein antibodies was observed in chickens inoculated with a regular dose of the inactivated vaccine until two weeks after booster vaccination, which was performed three weeks after prime vaccination (Fig. 1B). The inability of the inactivated vaccine to elicit early anti-IBV antibody responses in the systemic compartment was not due to an insufficient amount of antigen inoculated, as similar results were obtained in chickens immunized with the inactivated vaccine containing five times the amount of antigen (Supplementary Fig. 1). As assayed by flow cytometry (FCM), live-attenuated and killed vaccines significantly reduced the CD4/CD8 ratio to similar levels as soon as 4 days postimmunization (Fig. 1C). Moreover, the serum level of IFN-γ was persistently increased by both vaccines, but the difference was not significant (Fig. 1D), suggesting successful activation of cellular immune responses. The live-attenuated, but not killed, vaccine increased the T lymphocyte proportion in PBMCs (Fig. 1E), indicating that a higher-quality cellular immune response was initiated by the live-attenuated vaccine. To evaluate the antiviral effects conferred by vaccination, all chickens were infected with H120, the same strain used in vaccines, at a high dosage five weeks after live H120 prime vaccination or inactivated H120 booster vaccination. The live-attenuated vaccine successfully prevented viral infection with high-dose H120, as evidenced by the lack of viral shedding in oropharyngeal swabs throughout the observation period (Fig. 1F). In chickens immunized with the inactivated vaccine, viral shedding was clearly observed in oropharyngeal swabs from 4 days post infection (dpi) to 7 dpi and became undetectable at 10 dpi (Fig. 1F). Therefore, in our in vivo model, live-attenuated but not inactivated vaccine elicited successful anti-IBV adaptive immunity.

To obtain a comprehensive understanding of the underlying mechanism facilitating the distinct immune protection conferred by live-attenuated and killed vaccines, scRNA-seq data from the PBMCs of chickens at the onset of vaccination and at 4, 7, and 14 dpv were generated as indicated in Fig. 1G. In addition, considering the induction of antibodies recognizing the viral N protein by inactivated H120 from 14 days post-booster vaccination (35 days post-prime vaccination), the PBMCs of chickens at this timepoint were also subjected to scRNA-seq. To reduce the proportion of residual erythrocytes, a haemolysis step was performed before regular PBMC purification according to our previous scRNA-seq study of avian blood cells[34]. The purified PBMCs were composed mainly of lymphocytes, thrombocytes (a main component of chicken PBMCs), and monocytes as assayed by FCM (Fig. 1G).

The transcriptomes of 71,029 PBMCs were acquired, among which 66,778 passed quality control tests with medians of 1,091 counts and 567 genes per cell. A step-by-step high-resolution annotation with unsupervised clustering of all cellular transcriptomes, followed by cell type assignment with available known marker genes (the known marker genes detectible in scRNA-seq data) or properly generated references (when few marker genes are available for cell assignment) at each step, was established. A similar

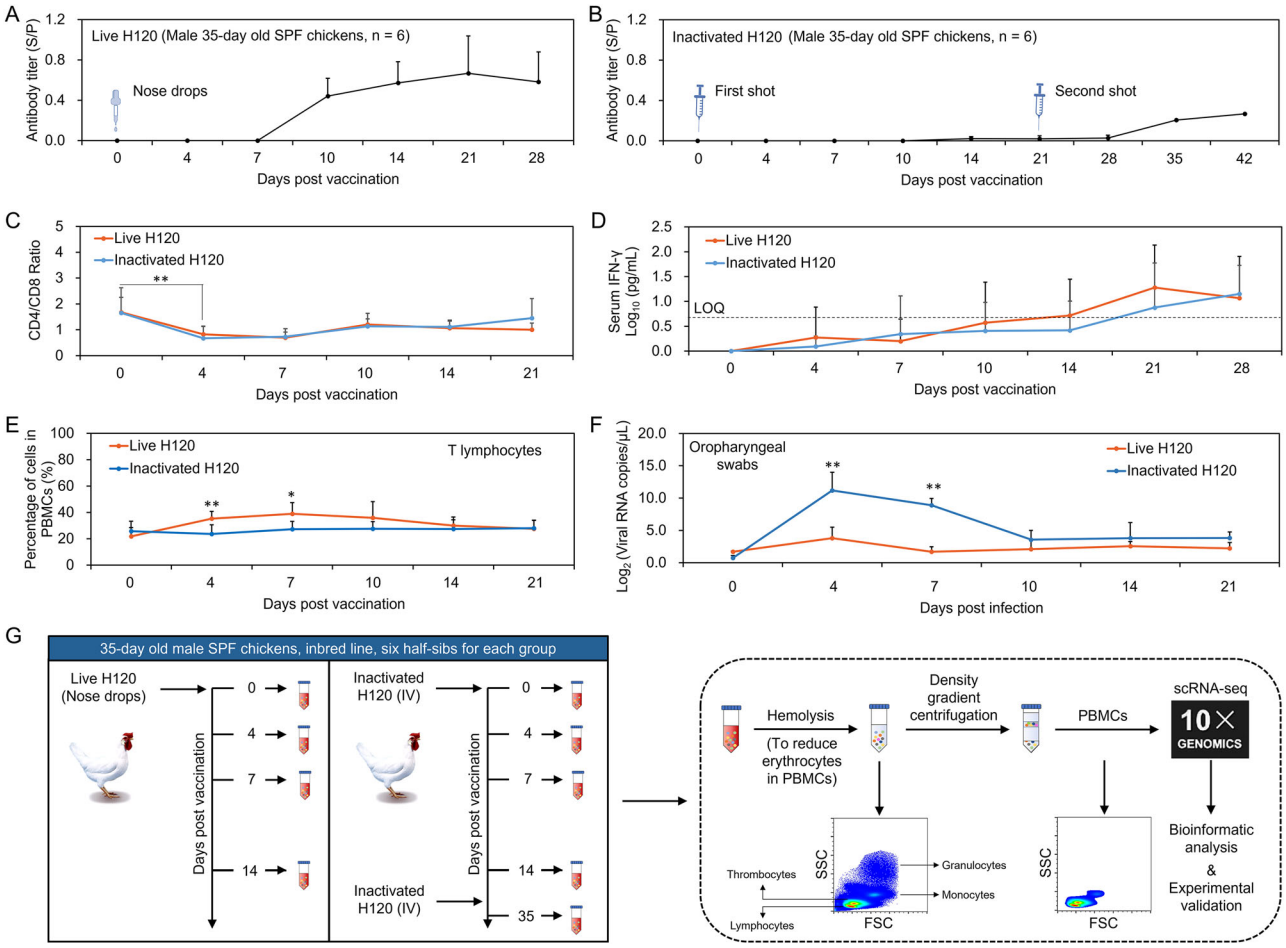

Fig. 1 | Characterization of animal model for avian coronavirus prime vaccination and illustration of the experimental workflow. A, **B** Detection of anti-N protein antibodies in chickens immunized with live-attenuated (**A**) or inactivated H120 (**B**). **C** CD4/CD8 ratio of peripheral T lymphocytes was assayed by flow cytometry (FCM). **D** Detection of serum IFN-γ by ELISA. LOQ: limit of quantification. **E** The proportion of $CD8^+$ T lymphocytes in PBMCs was assayed by FCM. **F** Oropharyngeal swabs were collected at the indicated timepoints. The number of viral RNA copies per microliter was detected by absolute qPCR. **G** Illustration of the experimental workflow. The two FCM plots are representative FSC vs. SSC plots of the blood samples collected at the indicated step of PBMC purification without gating. Data in **A**–**F** are presented as the mean ± SD (n = 6). Asterisks indicate a significant difference (*, $p < 0.05$; *, $p < 0.01$).

strategy for cell-type assignment was used in this study. Globally, unsupervised cell clustering using Seurat (version 4.1.0) identified 22 clusters, as shown in the 2D space by t-distributed stochastic neighbour embedding (t-SNE) (Fig. 2A). The cells were then manually annotated based on their expression of known marker genes (Fig. 2B) in combination with the correlation analysis of these clusters as presented in a clustering tree generated by clustree (version 0.4.4) using transcriptional profiles (Fig. 2C). After haemolysis and subsequent density gradient centrifugation (Fig. 1G), erythrocytes, the main impurities in avian PBMC preparations, were reduced to a small fraction of the cells. High transcription levels of four classic erythrocyte markers, HBA1, HBAD, HBBA, and SLC4A1, were observed only in clusters (C) 8, 16, and 18, all of which originated from C3 at a resolution of 0.01, suggesting that these three clusters consisted of residual erythrocytes; these clusters were removed from subsequent analysis. In contrast to mammalian platelets (thrombocytes), avian thrombocytes are nucleated cells, and abundant thrombocytes are present in purified avian PBMCs. The thrombocyte markers ITGAV and ITGB3 were expressed at high levels in C1, 2, 4, and 12, all of which originated from C1 at a resolution of 0.2; therefore, these four clusters were assigned as thrombocytes. The genes encoding class II histocompatibility antigen, BLB1 and BLB2, were highly expressed in four clusters, C9, 11, 13, and 21. Among these clusters, the B-cell markers BCL11A, SWAP70, PAX5, CD79B, and Bu1 were expressed at high levels in C9 and C13, both of which originated from C5 at a resolution of 0.6, and these cells were assigned as B lymphocytes. The monocyte/macrophage markers TLR4 and MAFB were enriched in C11, and the dendritic cell markers CADM1, FLT3, and XCR1 were enriched in C21; these two clusters were assigned as monocytes/macrophages and dendritic cells, respectively. C3, 5, 6, 7, 10, 14, 15, and 17 expressed CD4, CD28, CD8A, CD8BP, TCR gamma TARP and ZAP70 and were assigned as T lymphocytes. Given the expression of the markers of resting natural killer (NK) cells CLSPN, TOP2A, and ASPM and the markers of activated NK cells GNLY and XCL1, C14 and C15 may also be composed of NK cells. Considering the high expression of CD3D in C20, this cluster was also assigned as a T lymphocyte cluster.

Both live and inactivated H120 altered the composition of PBMCs greatly but at different rates and in different patterns. As shown by clustering analysis (Fig. 2D), the PBMC composition of individuals immunized with the live-attenuated vaccine formed clusters far from those of the mock group as early as 4 dpv, whereas the PBMC composition of individuals immunized with the inactivated vaccine shifted more slowly within the first week post vaccination. However, unexpectedly, the PBMC compositions of both vaccination groups gathered in the same cluster at 14 dpv, and this composition remained unchanged in the killed vaccine group at 35 dpv, indicating that this composition was stable (Fig. 2D). These data suggest that the two vaccines ultimately reshaped the host PBMC composition to the same state, which was completely different from that at the onset of vaccination. However, the processes through which live and inactivated vaccines directed PBMCs into this cellular composition were distinct. A great discrepancy in

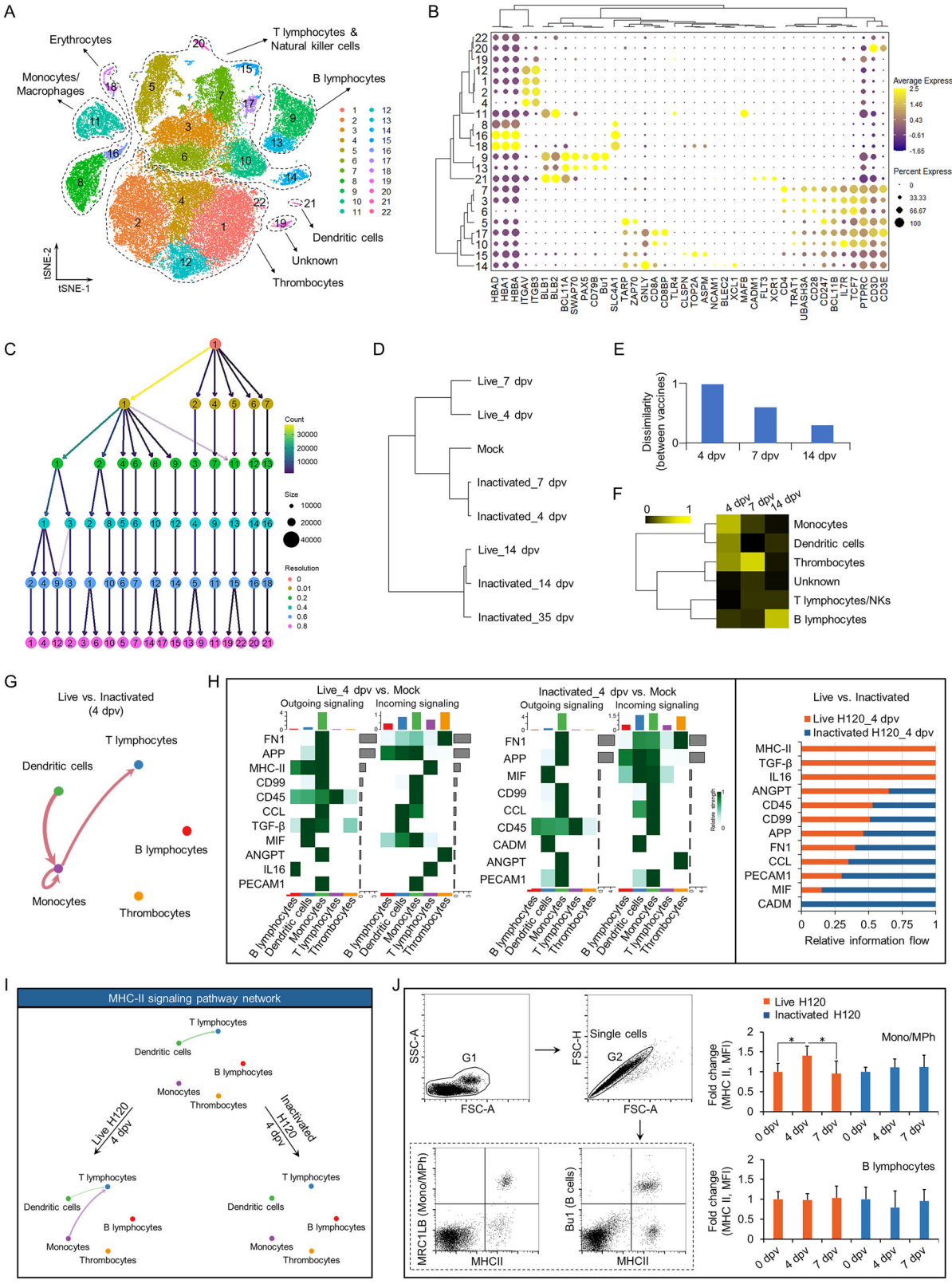

PBMC composition between chickens immunized with live-attenuated and inactivated vaccines was observed at 4 dpv, with a correlation coefficient (r) of only 0.01 (Fig. 2E). Moreover, the correlation of PBMC composition between the two groups increased over time, with r values of 0.35 and 0.70 at 7 and 14 dpv, respectively (Fig. 2E), indicating the importance of the discrepancies within the first week post vaccination. Comparisons of each type of PBMC between the two types of vaccines revealed that the substantial difference in PBMC composition within the first week after vaccination was contributed mainly by the distinct transitions of monocytes/macrophages, dendritic cells, and thrombocytes (Fig. 2F).

To understand the biological significance of the distinct transition patterns of innate immune cells directed by the two types of vaccines in the

Fig. 2 | Distinct dynamic PBMC landscapes upon prime vaccination with live-attenuated or inactivated IBV vaccine. A t-distributed stochastic neighbour embedding (t-SNE) clustering of PBMCs from all chickens with or without prime IBV vaccination. Cells of each cluster are labelled by different colours. **B** Dot plots of the expression of chicken immune cell markers. **C** Clustering tree of PBMCs generated by clustree (version 0.4.4) using transcriptional profiles. **D** Hierarchical clustering of chicken PBMC composition upon vaccinations. **E** Dissimilarity in PBMC composition between chickens immunized with live-attenuated H120 and those immunized with inactivated H120. **F** Hierarchical clustering of the differences of chicken PBMC compositions between inoculations with live or inactivated H120. **G** Circle plots presenting the comparison of cell–cell communication among PBMCs between chickens immunized with live-attenuated or inactivated H120 at 4 dpv. Different colours represent different cell types and edge width is proportional to the communication probability. Arrows indicate direction (source: target). Red arrow indicates the up-regulation. **H** Heatmap in the left panel presenting the significant ligand–receptor pairs between each cell type at 4 dpv (vs. Mock). Right panel presenting the comparison of pan-cell type signalling networks between live-attenuated and inactivated vaccine groups at 4 dpv. **I** Circle plots presenting the network centrality analysis of MHC class II signalling pathway. Different colours represent different cell types and edge width is proportional to the communication probability. Arrows and edge colour indicate direction (source: target). **J** The expression of MHC class II on the surfaces of monocytes and B lymphocytes was detected by FCM, and the data were used to calculate the number of changes. Left panel: gating strategy; right panel: statistical results are presented as the mean ± SD (n = 6), asterisks indicate a significant difference (*, $p < 0.05$). dpv: days post vaccination.

initiation of adaptive immune responses, cell-cell communication analysis was conducted using CellChat (version 1.4.0) with chicken-human orthologous genes (Ensembl BioMart)[35]. At 4 dpv, T lymphocytes received enhanced signals from dendritic cells and monocytes upon live virus vaccination, indicating that T lymphocyte activation by antigen processing cells (APCs) was the main biological process promoted by live H120 at 4 dpv (Fig. 2G). However, this communication between T lymphocytes and APCs was much weaker in the inactivated vaccine group. The specific signalling of cell-cell communication pathways between PBMCs upon vaccination are presented and compared in Fig. 2H. Among these signalling pathways, MHC class II signalling was transduced completely oppositely by live-attenuated and inactivated vaccines (Fig. 2H, I). The transduction of MHC class II signalling was enhanced at 4 dpv by the live-attenuated vaccine, and the main source of this signalling was switched from dendritic cells to monocytes. In chickens immunized with inactivated H120, the transduction of MHC class II signalling from APCs to T lymphocytes was halted at 4 dpv. For validation purposes, the expression levels of MHC class II molecules on the surfaces of APCs, including monocytes/macrophages and B lymphocytes, were detected by FCM. There were no detectable dendritic cells for FCM analysis of MHC class II expression in blood PBMCs. MHC class II expression was increased by live-attenuated H120, but not by inactivated H120, on the surfaces of monocytes at 4 dpv (Fig. 2J). No change in MHC class II expression was found on the surface of B lymphocytes upon vaccination. Considering the previously reported correlation between monocyte/macrophage MHC class II expression and IBV protection in live IBV-vaccinated MHC inbred chicken lines[36], the APC preference revealed here may play an important role in IBV prime vaccination.

In vivo dynamics of APCs upon IBV prime vaccination

Next, the transitions of monocytes/macrophages and dendritic cells upon vaccination with live-attenuated or inactivated vaccines were analysed. Unsupervised cell clustering grouped the 2359 monocytes/macrophages into six subclusters (MC1-6; Fig. 3A). Upon vaccination, the proportion of monocytes in PBMCs declined significantly and rapidly from 4 dpv in response to both the live-attenuated and inactivated vaccines, with no difference between the groups throughout the observation period (Fig. 3B). However, the composition of monocytes in birds immunized with live-attenuated vaccine changed dramatically as soon as 4 dpv, which was not observed in the killed vaccine group (Fig. 3C). In addition, the two types of vaccines shifted monocytes/macrophages to similar final compositions but in completely different ways, as shown by pseudotime analysis via Monocle3 (version 1.0.0) (Fig. 3D). The live-attenuated vaccine successfully triggered the APC function and antiviral innate immune responses of monocytes (MC3) at 4 dpv and shifted monocytes/macrophages to a state with high glucose and fatty acid metabolism (MC2) at 7 dpv according to the signalling pathways enriched by the module genes of each subcluster (Fig. 3D). The monocyte/macrophage state moved in a different direction upon vaccination with inactivated H120, and the proportion of MC4 cells, which featured enhanced focal adhesion and cell migration, increased together with almost complete depletion of MC3 cells at 4 dpv.

Human conventional dendritic cells (cDCs) consist of two subsets, known as type 1 (cDC1) and type 2 cDCs (cDC2)[37–39]. Our analysis revealed 110 dendritic cells, which were also defined as two subclusters, DC1 and DC2, by the FindClusters function in Seurat 4.1.0 (Fig. 3E). DC1 expressed high levels of 20 marker genes, including XCR1, a marker of human cDC1[37], and antigen-presenting-related molecules, such as MHC class II molecules BLB1/2 and coactivator CD80, suggesting its APC function (Fig. 3F, G). DC2 featured high transcription levels of five marker genes, including *IL6R* (Fig. 3F). Considering recent literature showing no evidence of cDC2 in chickens and the lack of definitive markers[40–42], DC2 was reclassified to as "inflammatory DC-like cells" rather than the avian counterpart of human cDC2 cells in chickens. Both vaccines shifted the composition of dendritic cells in PBMCs as early as 4 dpv but in different manners: the inactivated vaccine mainly increased the proportion of DC1 cells, while the live-attenuated vaccine mainly increased the proportion of DC2 cells (Fig. 3F). TGF-β signalling has been shown to be required for the maintenance of DCs and to be one of the determinants of APC preference during lymphocyte activation[43,44]. In line with the transducing patterns of MHC class II signalling, TGF-β signalling was also differentially transduced upon the administration of the two vaccines (Fig. 3H). Dendritic cells in the live-attenuated vaccine group received constant TGF-β signalling from B lymphocytes, thrombocytes, and monocytes/macrophages, which was halted by inactivated vaccine administration at 4 dpv (Fig. 3H). Consistent with the different transductions of TGF-β signalling in the two groups, the serum level of TGF-β1 was increased by the live-attenuated vaccine as soon as 4 dpv but was not changed by the inactivated vaccine as assayed by ELISA (Fig. 3I). In addition, the transcription levels of TGF-β receptors were significantly greater in DC2 (Fig. 3J). As summarized in Fig. 3K, the live attenuated vaccine preferred monocytes as initial APCs by promoting the expression of MHC class II molecules in monocytes/macrophages and TGF-β receptors in dendritic cells, while the inactivated vaccine preferred dendritic cells as APCs by promoting the expression of MHC class II molecules and reducing the expression of TGF-β receptors in dendritic cells.

Chicken thrombocytes play roles in both innate and adaptive immune responses. Five subclusters (ThC1-5) were identified during the reclustering of the 21,384 thrombocytes, suggesting substantial cellular heterogeneity (Supplementary Fig. 2A). In line with the transition patterns of monocytes and dendritic cells, different vaccines triggered completely distinct thrombocyte transitions (Supplementary Fig. 2B, C). The main component of thrombocytes before vaccination was ThC1 featured activated innate immune responses and ThC4 featured higher level of translation (Supplementary Fig. 2B, C). Upon live H120 vaccination, the proportion of ThC4 reduced gametically, while ThC1 became the dominate component of thrombocytes at 4 and 7 dpv. Upon inactivated H120 vaccination, ThC1 largely disappeared and ThC4 was replaced with ThC3 which was feathered with gene enrichment in translation and ATP synthesis. At 14 dpv, the thrombocytes of both vaccination groups transited into the same cellular composition, with most thrombocytes transiting into ThC2, a cluster of thrombocytes with enhanced migration. Consistent with cell-cell communication analysis of the MHC class II (Fig. 2I) and TGF-β signalling pathways (Fig. 3H),

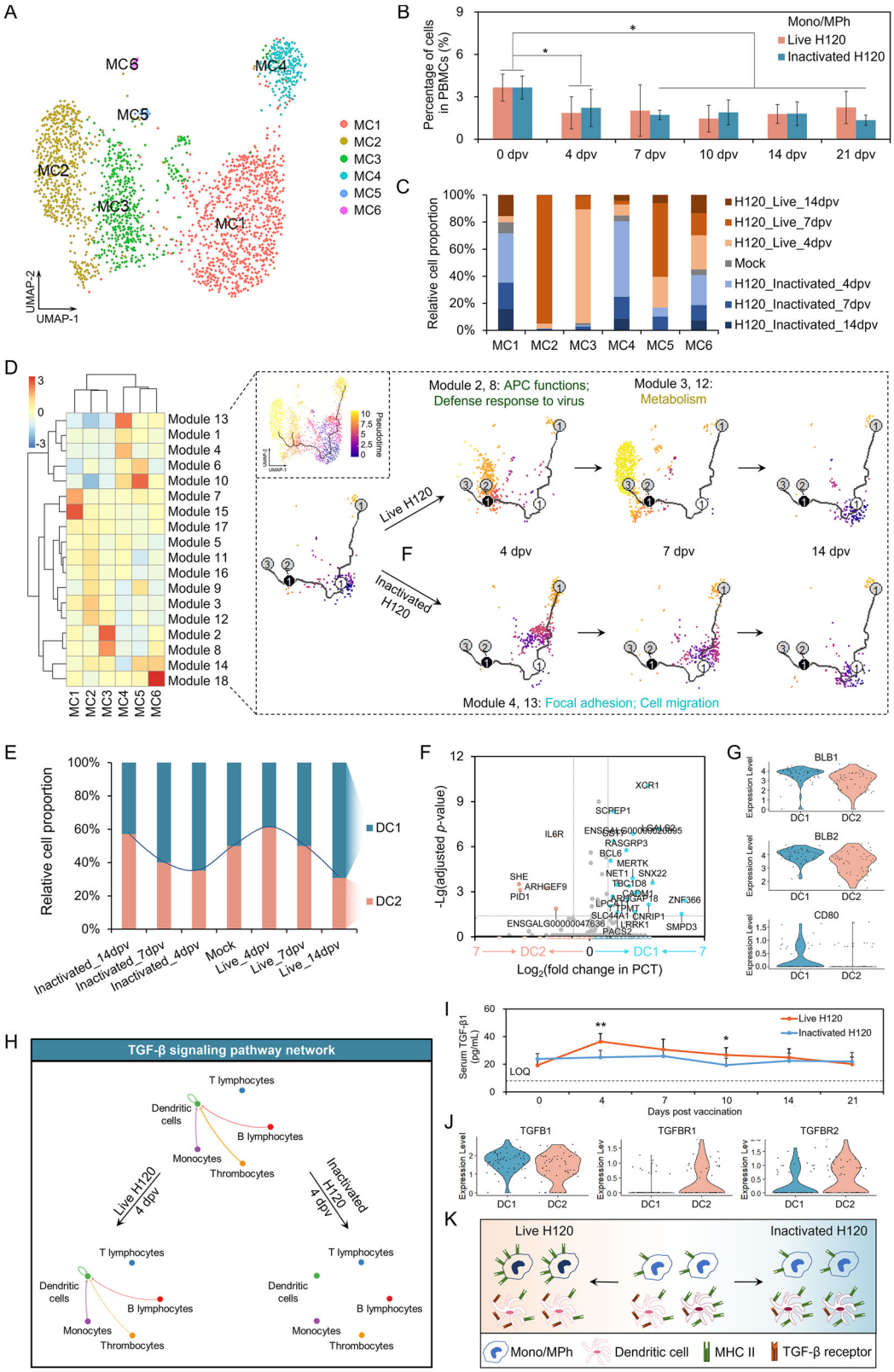

among the key genes of these two signalling pathways, only TGFB1 was highly expressed in thrombocytes (Supplementary Fig. 2D). However, no difference in the expression of TGFB1 between ThC1 and ThC3 was observed (Supplementary Fig. 2D). Thus, the contribution of thrombocytes to the differential induction of adaptive immune responses by live and inactivated H120 was not supported by our data.

Live-attenuated and inactivated vaccines reshape T lymphocyte composition in a similar manner but differ in terms of T lymphocyte expansion and TCR repertoire

To explore the biological significance of the APC preference for T lymphocyte activation upon live-attenuated and inactivated vaccine immunizations, 20,542 T lymphocytes were reclustered by unsupervised

Fig. 3 | In vivo dynamics of APCs upon IBV prime vaccination. A Uniform manifold approximation and projection (UMAP) clustering of monocytes from all chickens with or without prime IBV vaccination. Each subcluster is labelled with different colours. **B** The proportion of monocytes in PBMCs was assayed by FCM. **C**, **E** The relative proportion of each subcluster classified in monocytes (**C**) and dendritic cells (**E**). **D** Monocle analysis showing the transition of monocytes in pseudotime. Left: Heatmap of the differentially expressed genes (DEGs) along subclusters of monocytes; right: Schematic for the transition of monocyte composition upon vaccinations. **F** Volcano scatter plot showing the distribution of DC marker genes. y-axis: -$\log_{10}$ (adjusted p value); x-axis: $\log_2$ (fold change in PCT). Fold change in PCT, fold change in the percentage of cells highly expressing one specific marker gene in the designated DC cluster compared with that of those expressing the same gene in the other DC cluster. The most significant marker genes of DC1 and DC2 are highlighted in blue and red, respectively, and are identified by gene abbreviations. Other findings are presented as grey dots. **G**, **J** Expression of the key genes of MHC class II (**G**) and TGF-β (**J**) signalling pathways. **H** Circle plots presenting the network centrality analysis of TGF-β signalling pathway. Different colours represent different cell types and edge width is proportional to the communication probability. Arrows and edge colour indicate direction (source: target). **I** Detection of serum TGF-β1 by ELISA. LOQ: limit of quantification. **K** Schematic for differential APC preferences by live H120 and inactivated H120. Data in **B**, **I** are presented as the mean ± SD (n = 6). Asterisks indicate a significant difference (*, $p < 0.05$; **, $p < 0.01$). Mono: Monocytes; MPh: Macrophages; dpv: days post vaccination.

cell clustering, and 16 subclusters were identified, suggesting substantial cellular heterogeneity in T lymphocytes (TC1-16; Fig. 4A). Using 29 known chicken T lymphocyte and natural killer cell markers that were detectable in our data (Fig. 4B), in combination with the correlation analysis of T lymphocyte subclusters as presented in the clustering tree generated from the transcriptional profiles by clustree (version 0.4.4) (Fig. 4C), these 16 subclusters were defined as $CD4^+$ T lymphocytes (TC1, 2, 5, 6, 7, and 11), $CD8^+$ T lymphocytes (TC3 and 13), γδT lymphocytes (TC4, 8, 15, and 16), other T lymphocytes (TC9 and 14), and natural killer cells (TC10 and 12) (Fig. 4A). T lymphocyte activation upon vaccination was elucidated by cell-cell communication analysis tool CellChat (version 1.4.0), which identified communication between APCs and T cells via the MHC class II and CD80 (B7) signalling pathways at 4 dpv (Fig. 4D). As summarized in Fig. 4D, $CD4^+$ T cells were activated at 4 dpv by both live-attenuated and inactivated vaccines but using monocyte and dendritic cell subcluster 1 as APCs, respectively. Both vaccines activated TC1 and 7, while the live-attenuated vaccine also activated TC2 and 11, whose proportions were reduced only by the inactivated vaccine at 4 dpv (Figs. 4E, S3A). Conversely, TC11, the only subcluster with extensive activation of antiviral innate immune responses, was regulated by two types of vaccines (Figs. 4E, S3A, B). The activation of these $CD4^+$ T lymphocyte subclusters receiving MHC class II and B7 signals from APCs at 4 dpv was evidenced by their elevated expression of current known chicken T lymphocyte activation markers, including IL2RG, CD28, CD247, BCL11B, and TCRB (Fig. 4B, D). These markers, which are collectively associated with antigen recognition, co-stimulation, and clonal expansion in chickens, confirm a transition from naïve to antigen-responsive states. Consistent with what was observed for $CD4^+$ T-cell activation, live-attenuated and inactivated vaccine activated TC13, the $CD8^+$ T-cell subcluster expanded at 7 dpv in both groups (Fig. 4E and S3A), by monocyte and dendritic cell subcluster 1, respectively, via CD80 signalling pathway at 4 dpv (Fig. 4D). The two $CD4^+$ T lymphocyte subclusters, TC5 and TC6, and the $CD8^+$ T lymphocyte subcluster TC3 are most likely the avian counterpart of human stem-like memory T cells in chickens, because of their $CD28^+TCF7^{high}IL7R^{high}CD3^{low}$ phenotype (Fig. 4B) and lack of communication with APCs (Fig. 4D)[45–47]. Despite different APC preferences, the two types of vaccines generally reshaped the T lymphocyte composition in a similar manner (Fig. 4E). FCM analysis of $CD4^+$ and $CD8^+$ T lymphocytes, as indicated in Fig. 4F, revealed a reduction in the $CD4^+$ T lymphocyte proportion in response to the inactivated vaccine at 4 and 7 dpv and an increase in the $CD8^+$ T lymphocyte proportion in response to the live-attenuated vaccine at 7 dpv in PBMCs (Fig. 4G, H), suggesting that the two vaccines decreased the CD4/CD8 ratio through different mechanisms (Fig. 1C). In contrast to the increase in the proportion of $CD4^+$ T lymphocytes, the expression of CD4 on the cell surface of $CD4^+$ T lymphocytes was significantly reduced by the live-attenuated vaccine at 7 dpv (Fig. 4I). In line with the decreases in the CD4/CD8 ratio (Fig. 1C), the expression of CD8 on the cell surface of $CD8^+$ T lymphocytes was significantly promoted by both vaccines at 7 dpv (Fig. 4J). This was further evidenced by the increased proportion of T lymphocytes expressing high levels of CD8 on the cell surface (gate 4, G4) in both vaccination groups (Fig. 4K, L). Our FCM assay also observed a small fraction of $CD4^+CD8^+$ T lymphocytes and this proportion was not altered by vaccination (Supplementary Fig. 3C). However, the existence of $CD4^+CD8^+$ T lymphocytes was not supported by either other available scRNA-seq data of chicken immune cells or our present scRNA-seq data (Fig. 4B). Taken together, the similar promotion of serum levels of IFN-γ by both vaccines (Fig. 1D), the increased T lymphocyte proportion at 4 and 7 dpv by live-attenuated vaccine only (Fig. 1E) and the results mentioned above indicate that both APC preferences are capable of activating T lymphocytes and reshaping the T lymphocyte composition in a similar manner overall but differ in promoting T lymphocyte expansion.

APCs activate T lymphocytes through antigen presentation, which reshapes immune repertoires. Considering the discrepancy in antigen presentation among APCs due to their differential lysosomal proteolysis[48], the TCR repertoire was analysed. Single-cell-based immune repertoire analysis has been widely performed for human and mouse immune studies but is difficult to conduct for other species, including chickens, due to the limited annotation of their immune repertoires. We obtained 48,674,062 reads that could not be mapped to the chicken genome, 20,086,631 of which were found only in T lymphocytes (Fig. 4M). To compare the TCR repertoires of chickens immunized with live-attenuated and inactivated vaccines, the sequences of these 20,086,631 reads were mapped to current known chicken TCR repertoire data[49], which identified 45,462 reads representing 18,162 chicken TCR sequences (Fig. 4M). Only a few of these TCR reads were expressed in T cells at the onset of vaccination, and the number of TCR reads expanded dramatically and rapidly in T cells upon vaccination in both groups (Fig. 4N). T lymphocytes of the live-attenuated vaccine group had more TCR reads than did T lymphocytes of the inactivated vaccine group, while the numbers of TCR sequences were the same. Taking the higher $CD8^+$ T lymphocyte proportion in live vaccine group together (Fig. 4H), these findings suggest greater expansion of T-cell clones with specific TCR sequences upon live H120 vaccination. In addition, the distributions of these TCR sequences also differed between the two vaccination groups; 2,934 sequences (indicated as the "a" group) were highly expressed in the live-attenuated vaccine group, and another 1992 sequences (indicated as the "b" group) were highly expressed in the inactivated vaccine group, as shown by the heatmaps (Supplementary Figs. 3D, 4O), suggesting that different TCR repertoires were formed by the two vaccines.

Live-attenuated and inactivated vaccines activate B lymphocytes in different manners but yield similar BCR repertoires

As assayed by FCM, the proportion of B lymphocytes in PBMCs remained unaffected after prime vaccination in both groups (Fig. 5A). To investigate the dynamic transition of B lymphocytes upon vaccination, the 4255 B lymphocytes were reclustered by unsupervised cell clustering, and 11 subclusters were identified (BC1-11; Fig. 5B). Similar to what was observed for T lymphocytes, both vaccines reshaped B lymphocyte composition from 4 dpv and into the same state at 14 dpv, both of which were composed mainly of BC3, 4, and 5 (Fig. 5C). The two vaccines switched B lymphocyte composition in similar manners in general, except for BC4, 6, 7, and 10, whose proportions in B lymphocytes were oppositely regulated by live-attenuated and inactivated vaccines at 4 dpv (Figs. 5C, S4A). The transition of B lymphocytes was then characterized by trajectory analysis using Monocle3 (version 1.0.0) (Fig. 5D). The coexpression gene modules are

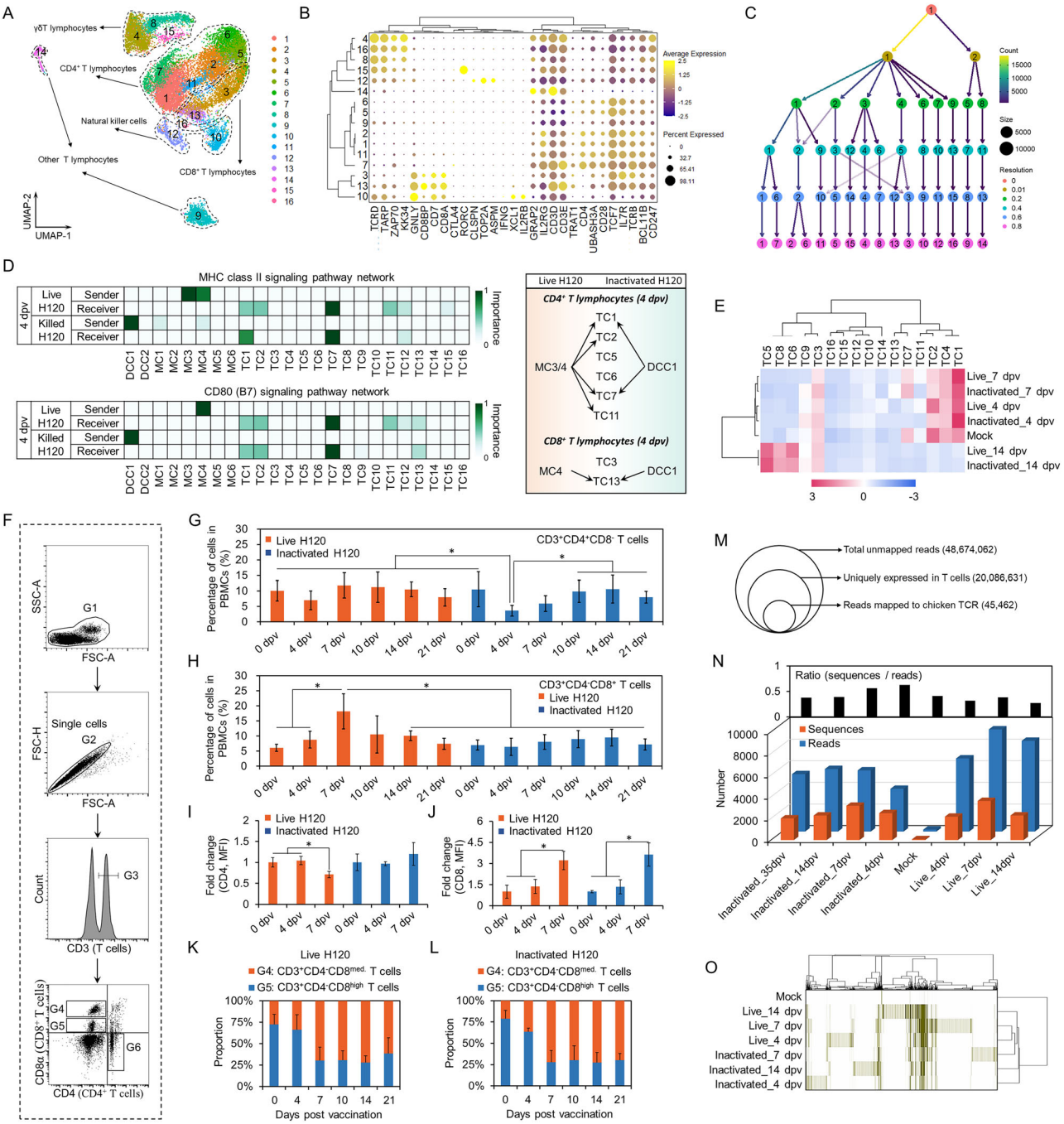

Fig. 4 | Live-attenuated and inactivated vaccines reshape T lymphocyte composition in a similar manner but differ in T lymphocyte expansion and TCR repertoires. A UMAP clustering of T lymphocytes from all chickens with or without prime IBV vaccination. Each subcluster of T lymphocytes is labelled by different colours. **B** Dot plots of the expression of T lymphocyte markers. **C** Clustering tree of T lymphocytes generated by clustree (version 0.4.4) using transcriptional profiles. **D** Heatmap shows the relative importance of each cell group based on the computed network centrality measures of MHC class II and CD80 signalling networks. Right panel: schematic for T lymphocyte activation. **E** Heatmap integrated with hierarchical clustering of the proportion of each T lymphocyte subcluster in PBMCs upon vaccination. Red indicates upregulation, blue indicated downregulation. **F–L** Dynamics of peripheral T lymphocytes upon vaccination assayed by FCM. Left panel: gating strategy (**F**); right panel: proportions of $CD3^+CD4^+CD8^-$ T lymphocytes (**G**) and $CD3^+CD4^-CD8^+$ T lymphocytes (**H**) in PBMCs, relative expression levels of CD4 (**I**) and CD8 (**J**) on the surfaces of T lymphocytes normalized to those of non-vaccinated groups, and relative proportions of $CD3^+CD4^-CD8^+$ T lymphocytes with regular or higher levels of cell surface CD8 upon immunization with live H120 (**K**) or inactivated H120 (**L**). **M** Schematic for reads selection. **N** Numbers of T lymphocyte-specific reads and sequences mapped to known chicken TCR among samples upon vaccination. **O** Heatmap presenting the distribution of TCR among samples. Data in F-L are presented as the mean ± SD (n = 6). Asterisks indicate a significant difference (*, $p < 0.05$). dpv: days post vaccination.

presented in a heatmap (Fig. 5D, left panel). As shown in Fig. 5C, the proportion of BC6 cells, which feature antiviral immune and APC functions (Fig. 5D, right panel), was increased upon live H120 vaccination but was reduced upon inactivated vaccination. In contrast, BC7, which featured high cell migration, apoptosis, nucleotide metabolism, and lysosome-related biological processes, and BC4, which featured biological processes related to B lymphocyte activation, expanded only in response to the inactivated vaccine (Figs. 5C, S4A). At 14 dpv, B lymphocytes in both groups transmitted to the same state, composed mainly of BC3, BC4, and BC5, which featured biological processes related to cellular senescence, ubiquitin

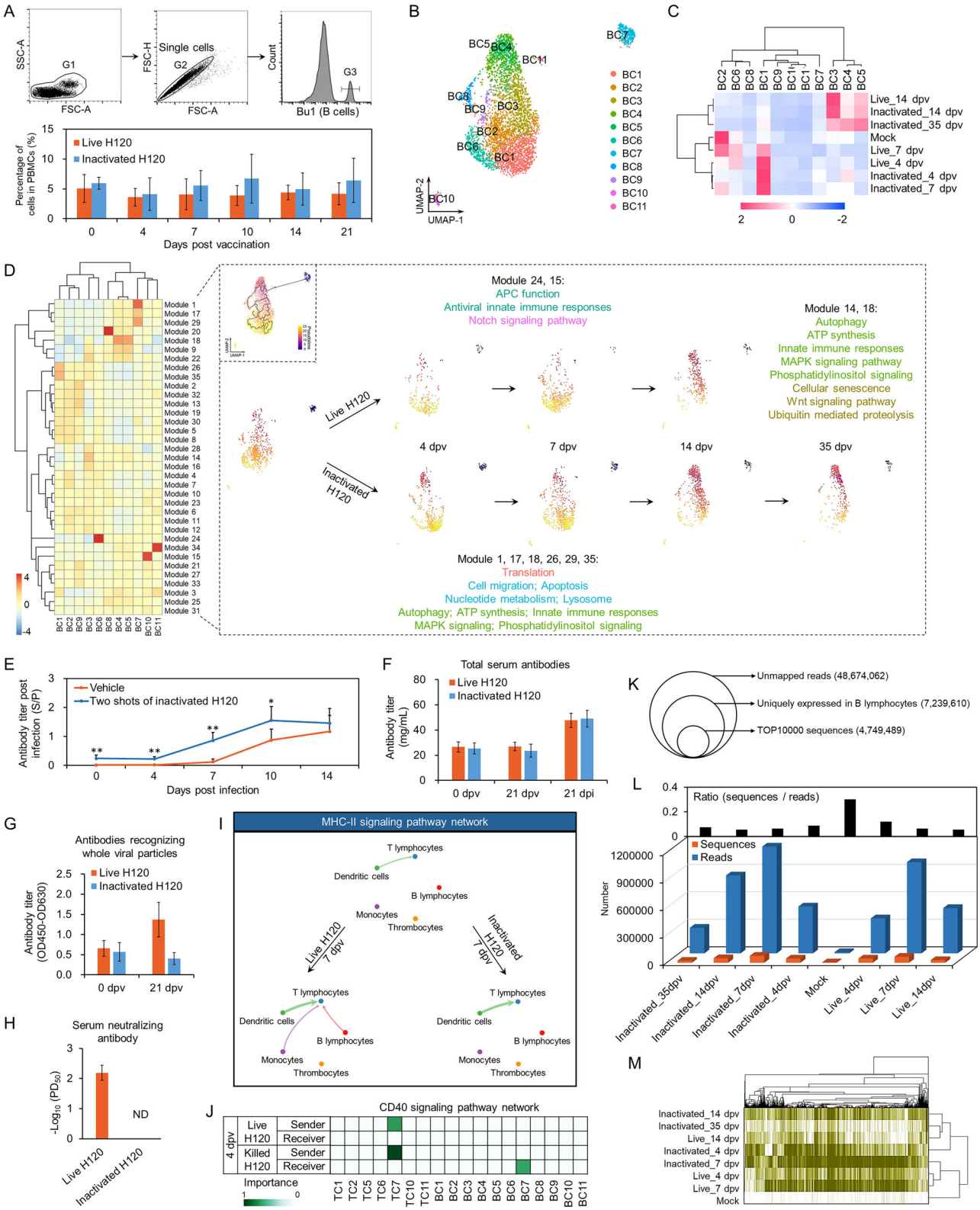

mediated proteolysis, and B lymphocyte activation and proliferation related signalling pathways, such as the Wnt signalling pathway, MAPK signalling pathway, autophagy, ATP synthesis, innate immune responses, and phosphatidylinositol signalling, suggesting successful activation of B lymphocytes by both vaccinations. The activation of B lymphocytes by the inactivated vaccine was demonstrated by the faster induction of serum antibodies specifically recognizing the viral N protein in chickens immunized with two shots of inactivated H120 upon infection with a high dose of H120 (Fig. 5E) and the significant promotion of total serum antibody levels by live-attenuated and inactivated vaccines to similar levels at 21 dpi (Fig. 5F), although neither serum antibodies specifically recognizing the viral N protein or whole viral particles nor serum neutralizing antibodies were induced by the inactivated vaccine at 21 days post prime vaccination (Figs. 1B, 5G, H). Our analysis identified distinct PBMC populations,

Fig. 5 | Live-attenuated and inactivated vaccines activate B lymphocytes in different manners but yield similar BCR repertoires. A Proportion of B lymphocytes in PBMCs upon vaccination. Upper panel: gating strategy; lower panel: the proportion of B lymphocytes in PBMCs was detected by FCM. **B** UMAP clustering of B lymphocytes from all chickens with or without prime IBV vaccination. Each subcluster of B lymphocytes is labelled by different colours. **C** Heatmap integrated with hierarchical clustering of the proportion of each B lymphocyte subcluster in PBMCs upon vaccination combining with clustering analysis. Red indicates upregulation, blue indicates downregulation. **D** Monocle analysis showing the transition of B lymphocytes in pseudotime. Left: Heatmap of the differentially expressed genes along subclusters of B lymphocytes; right: Schematic for the transition of B lymphocyte composition upon vaccination. **E** Detection of anti-N protein antibodies after infection in chickens immunized with two doses of inactivated H120 and chickens without vaccination (Vehicle). **F** Detection of total serum antibody. **G** Detection of total serum anti-H120 antibody. **H** Detection of serum neutralizing antibody. **I** Circle plots presenting the network centrality analysis of MHC class II signalling pathway. Different colours represent different cell types and edge width is proportional to the communication probability. Arrows and edge colour indicate direction (source: target). **J** Heatmap shows the relative importance of each cell group based on the computed network centrality measures of CD40 signalling network. **K** Schematic for reads selection. **L** Numbers of B lymphocyte-specific reads and sequences upon vaccination. **M** Heatmap presenting the distribution of putative BCR among samples. Data in **A** and **E**–**H** are presented as the mean ± SD (n = 6). Asterisks indicate a significant difference (*, $p < 0.05$; **, $p < 0.01$). d*p*v days post vaccination, dpi days post infection, ND not detectable.

including T lymphocytes, B lymphocytes, monocytes, dendritic cells, and thrombocytes, which may play crucial roles in the establishment of humoral immune responses following prime vaccination. To understand the different humoral immune responses triggered by live-attenuated and inactivated vaccines, B lymphocyte activation upon vaccination was elucidated by cell-cell communication analysis of these PBMC populations using CellChat (version 1.4.0). In line with the transition of B lymphocytes to the APC state upon vaccination with live H120 (Fig. 5D), MHC class II signalling from B to T lymphocytes was observed at 7 dpv in the live-attenuated vaccine group but not in the inactivated vaccine group (Fig. 5I). In fact, in addition to the fast activation of T lymphocytes through monocytes, live H120 triggered the MHC class II signalling pathway between T lymphocytes and all major APCs at 7 dpv, indicating more complete activation of T lymphocytes elucidated by the live-attenuated vaccine.

In addition to the T lymphocyte-dependent pathway, mammalian B lymphocytes can also be activated in a T lymphocyte-independent manner through direct stimulation by antigens such as polysaccharides, LPS, and other repetitive antigens, as well as through direct or indirect interactions with APCs[50]. Network analysis of CD40 signalling pathways between $CD4^+$ T cells and B cells revealed communication between $CD4^+$ T-cell subcluster TC7 and B-cell subcluster BC7 at 7 dpv in the killed vaccine group but not in the live-attenuated vaccine group (Fig. 5J), suggesting that live-attenuated and inactivated IBV vaccines initially activated B lymphocytes in T-cell-independent and T-cell-dependent manners, respectively. Considering the different TCR repertoires formed by live-attenuated and inactivated vaccines, the B lymphocyte repertoire was also analysed. Although chicken B lymphocyte repertoire data are currently unavailable, 7,239,610 unmapped reads specifically expressed in B lymphocytes were analysed (Fig. 5K). To minimize background noise, only the 4,749,489 reads of the top 10,000 sequences according to the read number of each sequence were used to analyse the distribution of the putative BCR repertoire. Similar to the distribution of TCR sequences, a few putative BCR reads were expressed in B cells at the onset of vaccination, while the number of BCR reads expanded dramatically and rapidly upon vaccination in both groups and peaked at 7 dpv (Fig. 5L). The ratio between the numbers of sequence and reads decreased rapidly after vaccination in both groups, suggesting the enrichment of reads in specific B-cell clones by both vaccines. However, different from those of the TCR repertoires, both the numbers of reads and sequences of BCR were greater in the inactivated vaccine group, suggesting that a broader BCR repertoire was formed by the inactivated vaccine through DC-mediated T lymphocyte-dependent B lymphocyte activation because of the similar B lymphocyte composition and proportions in the PBMCs of the two vaccination groups (Fig. 5L and Supplementary Fig. 4B). Furthermore, similar distributions of potential BCR sequences were observed between the two vaccine groups in general, as shown by the heatmaps (Fig. 5M and Supplementary Fig. 4B). The BCR repertoire formed by the live-attenuated vaccine at 14 dpv and that formed by the inactivated vaccine at 35 dpv when viral-specific serum antibodies had been induced were closely clustered together. This observation suggests that similar final BCR repertoires are formed by both vaccines, but the determination and expansion of optimized BCR clones are delayed by the inactivated vaccine compared with those driven by the live-attenuated vaccine. Thus, inactivated vaccines most likely delay the expansion of optimized BCR clones and subsequent virus-specific antibody production by forming a broader BCR repertoire.

The APC preference of live-attenuated IBV vaccine is not specific to vaccine modality

To understand whether the APC preference and the manner of subsequent lymphocyte activation upon live H120 prime vaccination is a live-attenuated vaccine-specific mechanism or common for effective vaccination in chickens, 35-day-old SPF male chickens immunized with live or inactivated low pathogenic avian influenza virus H9N2 were utilized as a model for comparison. Inactivated H9N2 induced HI antibodies successfully at 14 dpv, although this effect occurred one week later than that of live H9N2, and peaked at 21 dpv (Fig. 6A). Inoculation with inactivated H9N2 increased the level of blood IFN-γ constantly until 28 dpv, while the blood IFN-γ concentration induced by live H9N2 reached an equally high peak but more rapidly at 4 dpv and then decreased slowly thereafter (Fig. 6B). Thus, both live and inactivated H9N2 successfully induced HI antibodies and elevated blood IFN-γ concentrations under the present experimental conditions. Samples for scRNA-seq were collected as described in Fig. 1 at the time points indicated in Fig. 6A. A total of 55,819 PBMCs passed quality control tests, with medians of 991 counts and 503 genes per cell. Globally, unsupervised cell clustering using Seurat identified 24 clusters, as shown in 2D space by t-SNE (Fig. 6C). Cells were annotated as introduced in Fig. 2 (Fig. 6C, D). Live and inactivated H9N2 altered PBMC composition rapidly and dramatically in similar patterns in general, except for the PBMC composition elicited by live H9N2 at 4 dpv (Fig. 6E), indicating the importance of this discrepancy at 4 dpv in the rapid initiation of humoral immune responses by live H9N2. The activation of $CD4^+$ T lymphocytes was explored by network analysis, which revealed that $CD4^+$ T lymphocytes received signals from monocytes/macrophages, B lymphocytes, and $CD8^+$ T lymphocytes but not from dendritic cells or thrombocytes in both groups at 4 dpv (Fig. 6F). Further analysis of the transduction of MHC class II signalling suggests monocytes/macrophages as the main APCs during the activation of $CD4^+$ T lymphocytes in both groups, and B lymphocytes seemed to act as the secondary source of MHC class II signalling (Fig. 6G). At 7 dpv, the inoculation of live H9N2 mobilized all APCs to activate $CD4^+$ T lymphocytes through MHC class II signalling and stimulated dendritic cell switching to the dominant cell type. Similar to what we observed during $CD4^+$ T lymphocyte activation by IBV vaccines (Fig. 4), MHC class II signalling was not observed in the inactivated H9N2 group at 7 dpv (Fig. 6G). Thus, the APC preference of the live-attenuated IBV vaccine is common for the effective initiation of satisfactory antiviral immune responses by both the live IBV vaccine and inactivated AIV vaccine, during which MHC class II signalling from dendritic cells is not necessary. Furthermore, the low effectiveness of inactivated IBV in the initiation of early humoral immune response is antigen-determined, as simultaneous vaccination with inactivated H9N2 and H120 not only failed to induce antibody recognition of IBV but also impaired the induction of antibodies against AIV (Fig. 6H, I).

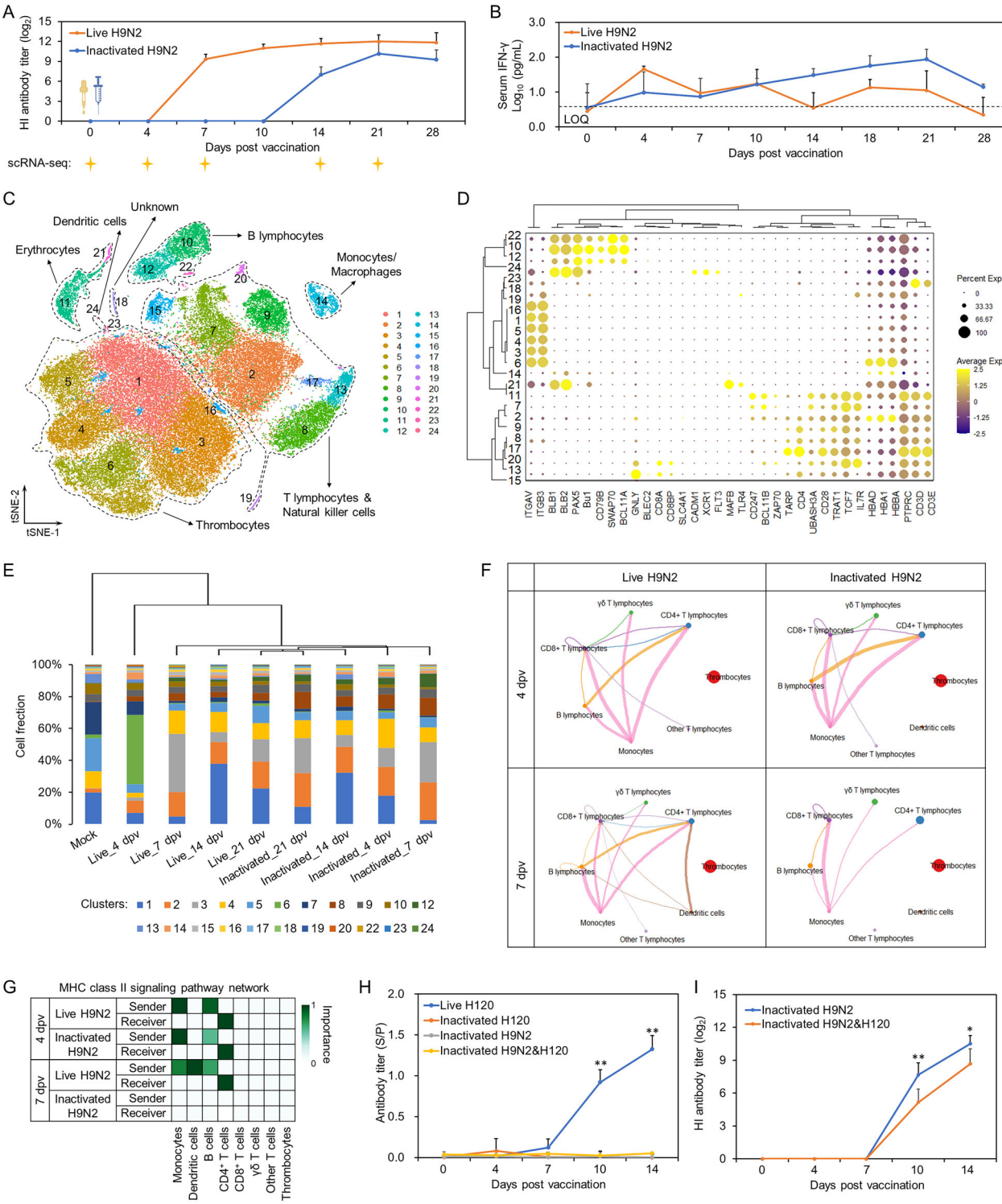

Fig. 6 | Dynamic transcriptomic landscape of chicken PBMCs upon prime avian influenza vaccination. A Detection of hemagglutination inhibition (HI) antibody. **B** Detection of serum IFN-γ. **C** t-SNE clustering of PBMCs from all chickens with or without prime AIV vaccination. Cells of each cluster are labelled by different colours. **D** Dot plots of the expression of chicken immune cell markers. **E** Hierarchical clustering of chicken PBMC composition upon vaccinations. **F** Circle plots presenting the number of interactions among PBMCs. Different colours represent different cell types. Circle sizes are proportional to the number of cells in each cell group and edge width represents the number of interactions. **G** Heatmap showing the relative importance of each cell group based on the computed network centrality measures of MHC class II signalling network. **H** Detection of anti-N protein antibodies after immunization with live H120, inactivated H120, inactivated H9N2, or co-immunization with inactivated H120 and H9N2. **I** Detection of HI antibody after immunization with inactivated H9N2, or co-immunization with inactivated H120 and H9N2. Data in **A**, **B**, **E**, and **I** are presented as the mean ± SD (n = 6). Asterisks indicate a significant difference (*, $p < 0.05$; **, $p < 0.01$). d*pv*: days post vaccination.

Discussion

Understanding the initiation of adaptive immune responses by prime vaccination is essential for the rational design of novel biosafe and effective vaccines. Although great efforts have been made to characterize host immune responses to coronavirus infection and vaccination, the current understanding of coronavirus prime vaccination is limited. IBV, the first coronavirus to be discovered, is not only a major threat to the global poultry industry but also a prototypical coronavirus. A single immunization with live-attenuated IBV vaccine is sufficient to provide host-satisfactory antiviral immune responses, while more than two doses of inactivated IBV vaccine are needed to induce pathogen-specific antibodies (Fig. 1A, B). Exploiting this comparison in our model, we constructed in vivo dynamic immune landscapes of prime vaccinations with live-attenuated and inactivated IBV vaccines at single-cell resolution. Unexpectedly, both vaccines altered the host immune landscape within the first week after immunization and reshaped PBMCs to the same immune activation composition by two weeks (Fig. 2D, E). The distinct immune responses elicited by live-attenuated and inactivated IBV vaccines correlate with differences in APC preferences and subsequent lymphocyte activation and immune repertoire formation. Despite the significant differences in vaccination efficacy and APC preference between groups immunized with live-attenuated or inactivated IBV vaccine, our data suggest that the preference of APCs is more strongly correlated with vaccine effectiveness than with vaccine modality in chickens, as prime vaccination with the inactivated AIV vaccine triggered comparable effective antiviral adaptive immune responses with the same APC preference as the live attenuated IBV (Figs. 3, 6). While the low effectiveness of inactivated IBV on immunity was antigen-determined (Fig. 6). Our findings highlight the importance of APC preference during prime vaccination in chickens. This observation may also be valuable for the rational design of safe and effective vaccines against coronaviruses in other species, including humans.

Live-attenuated vaccines have been extensively administered for the prevention and control of infectious diseases worldwide because they offer excellent protection[11–13]. However, growing evidence has led to great concerns about the biosafety risk of the use of live viruses for vaccines against a broad spectrum of viruses, such as polioviruses, coronaviruses, herpesviruses, and influenza viruses, as the use of live viruses may lead to the ongoing emergence of new variants[12,13,51,52]. The development of safe and effective IBV vaccines is restricted by the current limited understanding of the underlying mechanisms conferring the effective initiation of adaptive immunity against IBV infection, although many efforts have been made. This limitation may be because these previous studies focused mainly on the difference in lymphocyte composition after vaccination, which in fact is reshaped to identical composition via similar dynamics by live-attenuated and inactivated vaccines, as revealed by our analysis (Figs. 4–6). Instead, different APC preferences together with subsequent divergent immune activation and repertoires were identified between vaccines with distinct effectiveness. The live IBV vaccine seems likely to initiate adaptive immune responses more effectively than inactivated IBV vaccine by establishing a divergent antigen-recognizing spectrum of T lymphocytes and more efficient selection and expansion of premium B lymphocyte clones through APC preference different from that of the inactivated IBV vaccine rather than by driving the development of a different lymphocyte composition. This finding is consistent with previous findings that DC maturation and antigen presentation can be effectively induced by inactivated IBV but inhibited by live IBV[24–26]. However, the inactivated vaccine elicited broader initial BCR repertoire diversity than did the live vaccine during the first week post-vaccination (Figs. 5L, S4B), which might reflect distinct activation mechanisms: the inactivated vaccine's particulate antigen format could drive polyclonal B cell activation, whereas the live vaccine's replication-competent pathogen may focus the early response on immunodominant epitopes. However, both vaccines converged to similar overall BCR diversity, possibly due to affinity maturation and clonal selection, which refined the repertoire toward high-affinity antigen-specific clones. Unfortunately, further characterization of combinatorial diversity and tracking clonal lineages has been hindered due to the lack of comprehensive chicken B lymphocyte repertoire databases and tools for annotating gene segments of chicken BCR. The productive replication of IBV in monocytes and macrophages has been reported both in vivo and in vitro[28,29]. While its significance in chickens remains unclear. Our further analysis revealed the same APC preferences for the live IBV vaccine and inactivated AIV vaccine, both of which are capable of eliciting antiviral immune responses, suggesting that the preference of monocytes/macrophages as APCs rather than a vaccine modality-specific mechanism is common for effective prime vaccination in chickens and that the effectiveness of the inactivated IBV vaccine in inducing pathogen-specific humoral immunity at earlier stage after vaccination could be enhanced through APC modulation. The results of the present study indicate that, unlike those in humans and mice, monocytes/macrophages may be as capable as DCs in priming naïve T cells during prime vaccination in chickens. While our correlation analysis constructed the immune landscapes of chicken prime vaccination, we acknowledge that such associations do not confirm direct cellular crosstalk or causality. Functional validation, including co-culture assays, is essential for establishing these interactions mechanistically. However, technical limitations, such as the absence of tools to isolate or perturb the novel subclusters identified in our analysis, currently preclude such experiments in chickens. We have therefore prioritized complementary evidence, including activation marker expression, pathway enrichment, MHC II upregulation, and the dynamics of PBMC proportions, to contextualize these correlations. Future studies leveraging emerging chicken-specific reagents will address this gap.

The differences in the route of vaccination, which has important effects on the initiation of effective immune responses, may not explain the ineffectiveness of the inactivated IBV vaccine in inducing early pathogen-specific humoral immunity upon prime vaccination since the inoculation of inactivated AIV through the same route as that of inactive IBV achieved a humoral immune response as effective as that induced by the live-attenuated IBV vaccine (Figs. 1, 6). The low effectiveness of the inactivated IBV vaccine in initiating humoral immunity is antigen-determined, as simultaneous vaccination with inactivated H9N2 and H120 failed to improve the effectiveness of the inactivated IBV vaccine in humoral immunity (Fig. 6H, I). The inactivated IBV vaccine seems to contain certain components that can inhibit the initiation of adaptive immune responses, highlighting the importance of antigen selection when developing novel biosafe and effective IBV vaccines. In contrast to mammals, chickens do not have lymph nodes, and the site at which adaptive immune responses are initiated remains uncertain. The tracheal mucosal immune compartment is important for preventing the entry of IBV[11,22]; however, constant monitoring of immune dynamics is not supported by investigations of the tracheal mucosa. To explore immune dynamics upon infection or vaccination, the blood immune system, which can reflect systemic changes in immune responses, has been widely monitored by current scRNA-seq analysis in both humans and animals. This strategy was also employed by the present study to achieve time series observations under paired experimental design. However, the findings based on the analysis of systemic immune dynamics may not precisely reflect the main mechanisms and mediators of effective immune responses against IBV in the mucosal compartment of vaccinated chickens. The route of vaccination critically shapes immune outcomes for IBV vaccines[53,54]. For instance, mucosal routes directly target respiratory tissues, eliciting IgA and cell-mediated responses that block early viral entry[55,56]. In contrast, systemic routes prioritize humoral immunity but may lack mucosal protection[53]. These findings align with our observation that mucosal routes (live-attenuated vaccines) better control viral replication than inactivated vaccines via systemic routes (Fig. 1F). Recent advancements, such as gel-based administration, demonstrate prolonged antigen presentation and superior protection compared to traditional methods[55]. Our study compared live-attenuated (mucosal) and inactivated (systemic) vaccines to reflect real-world practices, ensuring relevance to field applications while acknowledging route-dependent immunological trade-offs[54,56]. Considering the importance of both the mucosal and systemic

compartments in effective immune responses against IBV, further investigations focus on the parameters identified in current analysis within the tracheal mucosal immune compartment are needed. The examinations of tracheal sections and tracheal swabs, rather than oropharyngeal swabs, are recommended for the evaluation of immune protection induced by IBV vaccines. To eliminate any influence other than vaccine modality and ensure that the data between groups immunized with different IBV vaccines were highly comparable, the same attenuated IBV strain was used at high dosages for homogenous restimulation in the present study. Notably, the difference in restricting the in vivo replication of H120 strain would not necessarily correlate with the protection from the challenge by a virulent strain, although the main conclusions of the present study would not be affected as chickens immunized with live-attenuated or inactivated IBV vaccines is a well-established comparative model for avian coronavirus prime vaccination. In the present study, male chickens were selected to reduce sex-based variability in immune responses. However, sex differences may significantly affect immune dynamics upon prime vaccination in chickens due to hormonal variability. Future single-cell transcriptomic analyses comparing these sex differences may provide more valuable information and improve our understanding of the mechanisms determining the efficacy of prime vaccination in chickens. While our study provides a comprehensive comparison of immune dynamics elicited by live-attenuated and inactivated vaccines, it is important to note that both formulations contain non-viral components that may independently influence immune responses. The lack of a parallel non-infectious vehicle control group prevents definitive discrimination between effects mediated by viral antigens and those triggered by other vaccine constituents. Future studies incorporating such controls will be essential to unravel these distinct contributions and refine vaccine design strategies.

One crucial step and current challenge for the analysis of scRNA-seq data from nonmodel animals is cell type assignment, due to the unavailability of high-quality reference genomes and to the lack of tools and platforms for subsequent validation and further functional analyses[47]. Our and others' previous scRNA-seq analyses of avian immune cells revealed that direct cell-type assignment for avian immune cells using orthologous genes in human and model animal databases is ineffective[34,57]. Therefore, a strategy combining the unbiased grouping of cells based on their transcriptional profiles and manual cell type annotation using currently known chicken immune cell markers conserved across different sequencing datasets and publications has been established for chicken immune cell type assignment and is wildly accepted by most scRNA-seq studies of avian immune cells[34,58–62]. However, some known chicken immune cell markers, such as CSF1R, the definitive marker for chicken monocytes and macrophages, are not present in scRNA-seq data. This may be due to either the different gene expression patterns of immune cells isolated from different tissues or the limited number of genes that scRNA-seq techniques can capture at the current stage. Therefore, further categorization of APCs using these known marker genes by methods such as RT-qPCR and FCM may improve the identification of specific subgroups of APCs conferring effective initiation of host adaptive immunity against IBV infection.

A comprehensive understanding of prime vaccination is essential for the rational design of novel biosafe and effective vaccines. Our present study provides single-cell in vivo dynamic immune landscapes of prime vaccination against two major respiratory infectious diseases in chickens and highlights the importance of APC preference in the effectiveness of vaccination. These findings may contribute to further investigations of the mechanisms underlying successful prime vaccination in birds. The single-cell transcriptomic data for 122,597 individual chicken PBMCs provided here could be a valuable resource for further comparative analysis across species.

Materials and methods

Ethics statement

The animal experiments and isolation of peripheral blood cells were approved by and performed in accordance with the ethical guidelines of the Animal Ethics Committee of Harbin Veterinary Research Institute (HVRI) of the Chinese Academy of Agricultural Sciences (approval no. 201204-03).

Experimental animals, virus, in vivo infection, and vaccination

Healthy 35-day-old BWEL specific-pathogen free (SPF) male chickens (Gallus gallus), an inbred line established and maintained at the Chinese State Resource Center of Poultry Laboratory Animals, were kept at the Laboratory Animal Science Department of Harbin Weike Biotechnology Development Company (ABSL-3, accredited by the China National Accreditation Service for Conformity Assessment), a state-owned enterprise subordinated to HVRI. The IBV H120 strain and AIV H9N2 strain were stored at the HVRI. These strains are propagated in SPF chicken embryos. Virus titre were calculated by the method of Reed and Muench and expressed as 50% embryo infectious dose (EID_{50})[63]. For live vaccine immunization, chickens were received 100 microliters (μL) of virus specimens at 10^4 EID_{50} per millilitre (mL) of live H120 or 100 μL of virus specimens at 10^6 EID_{50}/0.1 mL dose of live H9N2, respectively, through the nasal route. To eliminate any influence other than vaccine modality, H120, instead of a homologous virulent M41 strain, was used for preparing inactivated IBV vaccine. For inactivated vaccine immunization, H120 and H9N2 were killed with β-propiolactone (BPL) and used to make inactivated oil-emulsified vaccines. The birds received 300 μL of inactivated H120 at dose of 10^6 EID_{50}/0.1 mL through the subcutaneous injection route. A second shot of inactivated H120 was performed at the 21st. day post prime vaccination. For in vivo infection, the birds received 100 μL of virus specimens at 10^6 EID_{50}/0.1 mL dose of live H120 through the nasal route. To estimate the protection by vaccination, at five weeks post live H120 vaccination or the second shot of inactivated H120, all chickens received 100 μL of virus specimens at 10^6 EID_{50}/0.1 mL dose of live H120 through the nasal route, instead of other strains, to keep the data of all groups highly comparable. In all experiments, six half-sibs were used for each group. To achieve time series observations under paired experimental design, the data of non-vaccinated groups (at the onset of prime vaccination) were used as control groups for both live-attenuated and inactivated vaccine groups.

Virus shedding detection

To detect virus shedding, oropharyngeal swabs were collected from all chickens at indicated timepoints and then immersed in 1 mL of sterile PBS supplemented with antibiotics. Viral RNA was extracted from swab samples using RNA Miniprep kit (Axygen Scientific Inc, CA, USA), and subsequent absolute quantitative PCR (qPCR) detection was performed using the one-step primescript RT-PCR (Takara, Beijing, China) according to previous description[53]. The following absolute qPCR primers and TaqMan probe sequences targeting viral 3' untranslated region (UTR) were designed according to the complete genome of IBV strain H120 (ON350836.1). Forward primer: CTATCGCCAGGGAAATGTC; Reverse primer: GCGTCCTAGTGCTGTACCC; Probe: [FAM]CCTGGAAACGAACGG-TAGACCCT[TAMRA]. The standers of absolute qPCR were prepared by cloning the PCR products into the pMD18-T plasmid (Takara Biotechnology, Dalian, China) according to the manufacturer's instruction.

Serology detections

Serum samples were collected from all chickens at indicated timepoints. The levels of antibody specifically recognizing viral N protein, the most plentiful viral protein during viral replication, were determined using a commercial IBV enzyme-linked immunosorbent assay kit (NECVB, Harbin, China) by calculating the sample to positive (S/P) ratio[64]. Serum sample with S/P ratios less than or equal to 0.20 was considered negative; S/P ratio greater than 0.20 was considered positive. The levels of antibodies recognizing whole IBV virus were detected by ELISA using plates coated with sonicated H120 viruses. The levels of AIV neutralizing antibody were determined by detection of hemagglutination inhibition (HI) antibody. The levels of total serum antibody were quantified by ELISA using peroxidase conjugated rabbit anti-chicken Fc antibody (Cat# A9046, Sigma-Aldrich, Shanghai, China) in plates coated with each serum sample. The purified native chicken

IgY (Cat# bs-0310P, Bioss, Beijing, China) was used to prepare a standard curve. Serum IFN-γ and TGF-β1 levels were detected using Chicken IFN-γ ELISA kits (Mabtech, Stockholm, Sweden) and Chicken TGF-β1 ELISA kits (mlbio, Shanghai, China), respectively. For ELISA tests, the optical density in each plate was measured at 450 nm wavelength, and a reference wavelength of 630 nm used to subtract background signal.

Peripheral blood cell separation

The heparinized peripheral blood samples (10 mL per chicken) were taken from these chickens at indicated timepoints and transferred to laboratory for further isolation within one hour. Blood samples were firstly treated with erythrocyte lysis buffer (SolelyBio, Shanghai, China) to reduce the proportion of erythrocytes, according to our experience in avian blood immune cells preparation for single-cell sequencing, and then separated by density gradient centrifugation using a chicken lymphocyte isolation kit (Ficoll; Haoyang Biological Technology, Tianjin, China). Peripheral blood mononuclear cells (PBMCs), the cells in the middle white layer, were washed with RPMI 1640 culture medium (Gibco, Carlsbad, CA, USA) and adjusted the cell concentrations to 1×10^6 cells/ml for subsequent analysis.

Flow cytometry

PBMCs were first washed with PBS and adjusted the cell concentrations to $1{\times}10^6$ cells/ml for subsequent analysis. Cell viability was confirmed using Trypan Blue (Sigma-Aldrich, Shanghai, China). The cell viabilities of these samples were greater than 90%. Cells were stained with a cocktail of antibodies directed against CD3 (Cat# 8200-11, CT-3, APC), CD4 (Cat# 8210-02, CT-4, FITC), CD8α (Cat# 8390-09, EP72, PE), Bu1 (Cat# 8395-02, AV20, FITC), MRC1LB (Cat# 8420-09, KUL01, PE), MHCII (Cat# 8350-02, 2G11, FITC) purchased from SouthernBiotech (Birmingham, AL, USA) for 30 min at room temperature in the dark. Next, excess antibody was removed by washing with PBS. Then cells were resuspended in 0.5 mL PBS and acquired on a Cytomics FC 500 (Beckman Coulter Inc., CA, USA). Data were analyzed by FlowJo software v10 (Tree Star, Ashland, OR, USA).

Single-cell RNA sequencing

Sample preparation was performed in consistent with current published scRNA-seq studies for chicken immune cells with optimized experimental design[34,60,61]. Briefly, Balanced design was conducted by pooling PBMCs isolated from six half-sibs within the same group together with equal amounts of cells to reduce the variability effectively.

scRNA-seq of chicken PBMCs was performed by Annoroad Gene Technology Co., Ltd. One million cells were taken from each PBMCs and mixed. Then 10,000 pooled cells were processed following the user guide of Chromium™ Single Cell 3' Reagent Kits v3 involving the Chromium™ Single Cell Controller (10x Genomics, CA, USA) for constructing the libraries which were sequenced using Illumina HiSeq 2500 system. The cell viabilities of these samples were greater than 90%.

Single-cell transcriptome data analysis

Cell Ranger pipelines (version 3.0.1, https://github.com/10XGenomics/cellranger) were used to align complementary DNA reads to chicken reference (assembly: GRCg6a). More than 90% of the reads were mapped to the reference. A filtered unique molecular index (UMI) expression matrix was generated using default parameters. The expression matrix was normalized using the "cellranger aggr" function in the Cell Ranger. In accordance with the Cell Ranger pipelines and quality control standards, abnormal cells were uniformly filtered out based on their gene expression distribution. A cell was considered abnormal if any of the following criteria were met: (i) detected gene number < 200; (ii) detected gene number > 2500; and (iii) more than 10% of detected genes were mitochondrial genes. A "detected gene" is defined as any gene expressed in ≥ 3 individual cells at a level of UMI ≥ 1. Gene Ontology (GO) and KEGG pathway analysis was performed with DAVID (gene-enrichment analysis using EASE Score, a modified Fisher exact *p*-value, as the threshold)[65]. Raw RNA sequencing data were uploaded to the National Center for Biotechnology Information database under the accession number GSE220071 and GSE291364.

Clustering and pseudotime analysis

For cell clustering, unsupervised cell clustering using Seurat R toolkit (version 4.1.0, https://github.com/satijalab/seurat) was applied following its typical pipeline[66]. The cell composition landscape was visualized in 2D space using Uniform manifold approximation and projection (UMAP) or t-distributed stochastic neighbourhood embedding (*t*-SNE)[67,68]. Cell types were manually annotated based on the specific expression of currently known chicken immune marker genes[60–62,69–75]. Pseudotime analysis was performed using Monocle3 (version 1.0.0) and module genes were identified and annotated according to the typical pipeline provided (https://cole-trapnell-lab.github.io/monocle3/)[76]. Cell-cell communication analysis was conducted using CellChat R toolkit (version 1.4.0)[77] with chicken-human orthologous genes downloaded from Ensembl BioMart[35].

Statistical analysis

The SPSS software package (SPSS for Windows version 13.0, SPSS Inc., IL, USA) was used for all statistical analyses. All measurements were taken from distinct samples. Data obtained from several experiments are reported as the mean ± standard deviation (SD). The significance of differences between two groups was determined with two-tailed Student's t-test. One-way or two-way analysis of variances with Bonferroni correction was employed for multi-group comparison. For all analyses, a probability (p) value of < 0.05 was considered statistically significant.

Data availability

Raw RNA sequencing data were uploaded to the National Center for Biotechnology Information database under the accession number GSE220071 and GSE291364. All additional data included in this study are available from the corresponding authors upon request. No special code was reported in this paper.

Received: 1 July 2023; Accepted: 30 April 2025;
Published online: 18 May 2025

References

1. Terrier, O. et al. Influenza viruses and coronaviruses: knowns, unknowns, and common research challenges. *PLoS Pathog.* **17**, e1010106 (2021).
2. Liu, Y., Liu, J. & Shi, P. Y. SARS-CoV-2 variants and vaccination. *Zoonoses* **2**, 6 (2022).
3. Schalk, A. F. & Hawn, M. C. An apparently new respiratory disease in baby chicks. *J. Am. Vet. Med. Assoc.* **78**, 413–422 (1931).
4. Beaudette, F. & Hudson, C. Cultivation of the virus of infectious bronchitis. *J. Am. Vet. Med. Assoc.* **90**, 51–60 (1937).
5. Toro, H. Global control of infectious bronchitis requires replacing live attenuated vaccines by alternative technologies. *Avian Dis.* **65**, 637–642 (2021).
6. Cavanagh, D. Severe acute respiratory syndrome vaccine development: experiences of vaccination against avian infectious bronchitis coronavirus. *Avian Pathol.* **32**, 567–582 (2003).
7. Nefedova, E. et al. The infectious bronchitis coronavirus pneumonia model presenting a novel insight for the SARS-CoV-2 dissemination route. *Vet. Sci.* **8**, 239 (2021).
8. Quinteros, J. A., Ignjatovic, J., Chousalkar, K. K., Noormohammadi, A. H. & Browning, G. F. Infectious bronchitis virus in Australia: a model of coronavirus evolution—a review. *Avian Pathol.* **50**, 295–310 (2021).
9. Franzo, G. et al. Effect of different vaccination strategies on IBV QX population dynamics and clinical outbreaks. *Vaccine* **34**, 5670–5676 (2016).
10. Zhang, X., Guo, M., Zhao, J. & Wu, Y. Avian infectious bronchitis in China: epidemiology, vaccination, and control. *Avian Dis.* **65**, 654–658 (2021).

11. Legnardi, M., Tucciarone, C. M., Franzo, G. & Cecchinato, M. Infectious bronchitis virus evolution. *Diag. Control. Vet. Sci.* **7**, 79 (2020).
12. Han, Z. X. et al. A 15-year analysis of molecular epidemiology of avian infectious bronchitis coronavirus in China. *Infect. Genet Evol.* **11**, 190–200 (2011).
13. Zepp, F. Principles of vaccination. *Methods Mol. Biol.* **1403**, 57–84 (2016).
14. Vetter, V., Denizer, G., Friedland, L. R., Krishnan, J. & Shapiro, M. Understanding modern-day vaccines: what you need to know. *Ann. Med.* **50**, 110–120 (2018).
15. Li, J. X., Li, Z. P., Zhu, Y. W., Zhou, L. L. & Zhu, F. C. Evidence of the efficacy and the effectiveness of first generation COVID-19 vaccines in clinical trials and real-world studies. *Zoonoses* **2**, 30 (2022).
16. Chhabra, R., Chantrey, J. & Ganapathy, K. Immune responses to virulent and vaccine strains of infectious bronchitis viruses in chickens. *Viral Immunol.* **28**, 478–488 (2015).
17. Cook, J. K., Davison, T. F., Huggins, M. B. & McLaughlan, P. Effect of in ovo bursectomy on the course of an infectious bronchitis virus infection in line C White Leghorn chickens. *Arch. Virol.* **118**, 225–234 (1991).
18. Cook, J. K., Huggins, M. B. & Ellis, M. M. Use of an infectious bronchitis virus and Escherichia coli model infection to assess the ability to vaccinate successfully against infectious bronchitis in the presence of maternally-derived immunity. *Avian Pathol.* **20**, 619–626 (1991).
19. Chandra, M. Comparative nephropathogenicity of infectious bronchitis virus in bursectomized and nonbursectomized chickens. *Am. J. Vet. Res.* **49**, 831–834 (1988).
20. Darbyshire, J. H. & Peters, R. W. Humoral antibody response and assessment of protection following primary vaccination of chicks with maternally derived antibody against avian infectious bronchitis virus. *Res. Vet. Sci.* **38**, 14–21 (1985).
21. Gurjar, R. S., Gulley, S. L. & van Ginkel, F. W. Cell-mediated immune responses in the head-associated lymphoid tissues induced to a live attenuated avian coronavirus vaccine. *Dev. Comp. Immunol.* **41**, 715–722 (2013).
22. Okino, C. H. et al. Humoral and cell-mediated immune responses to different doses of attenuated vaccine against avian infectious bronchitis virus. *Viral Immunol.* **26**, 259–267 (2013).
23. Hilligan, K. L. & Ronchese, F. Antigen presentation by dendritic cells and their instruction of $CD4^+$ T helper cell responses. *Cell Mol. Immunol.* **17**, 587–599 (2020).
24. Lin, J., Wang, Z., Wang, J. & Yang, Q. Microarray analysis of infectious bronchitis virus infection of chicken primary dendritic cells. *BMC Genomics* **20**, 557 (2019).
25. Zuo, J. et al. The mechanism of antigen-presentation of avian bone marrowed dendritic cells suppressed by infectious bronchitis virus. *Genomics* **113**, 1719–1732 (2021).
26. Wu, Y. et al. IBV QX affects the antigen presentation function of BMDCs through nonstructural protein16. *Poult. Sci.* **102**, 102620 (2023).
27. de Geus, E. D. & Vervelde, L. Regulation of macrophage and dendritic cell function by pathogens and through immunomodulation in the avian mucosa. *Dev. Comp. Immunol.* **41**, 341–351 (2013).
28. Amarasinghe, A. et al. Infectious bronchitis corona virus establishes productive infection in avian macrophages interfering with selected antimicrobial functions. *PLoS One* **12**, e0181801 (2017).
29. Sun, X. et al. Analysis of chicken macrophage functions and gene expressions following infectious bronchitis virus M41 infection. *Vet. Res.* **52**, 14 (2021).
30. Wilk, A. J. et al. A single-cell atlas of the peripheral immune response in patients with severe COVID-19. *Nat. Med.* **26**, 1070–1076 (2020).
31. Xiong, L. et al. Online single-cell data integration through projecting heterogeneous datasets into a common cell-embedding space. *Nat. Commun.* **13**, 6118 (2022).
32. Chen, Y. J. et al. Single-cell RNA sequencing to decipher the immunogenicity of ChAdOx1 nCoV-19/AZD1222 and mRNA-1273 vaccines in patients with autoimmune rheumatic diseases. *Front. Immunol.* **13**, 920865 (2022).
33. Yoon, B. K. et al. The peripheral immune landscape in a patient with myocarditis after the administration of BNT162b2 mRNA vaccine. *Mol. Cells* **45**, 738–748 (2022).
34. Liang, Y. et al. Single-cell analysis of the in vivo dynamics of host circulating immune cells highlights the importance of myeloid cells in avian flaviviral infection. *J. Immunol.* **207**, 2878–2891 (2021).
35. Martin, F. J. et al. Ensembl 2022. *Nucleic Acids Res.* **50**, D988–D995 (2022).
36. Larsen, F. T. et al. Immunoprofiling of peripheral blood from infectious bronchitis virus vaccinated MHC-B chicken lines - Monocyte MHC-II expression as a potential correlate of protection. *Dev. Comp. Immunol.* **96**, 93–102 (2019).
37. Gardner, A. & Ruffell, B. Dendritic cells and cancer immunity. *Trends Immunol.* **37**, 855–865 (2016).
38. Sittig, S. P. et al. A comparative study of the T cell stimulatory and polarizing capacity of human primary blood dendritic cell subsets. *Mediators Inflamm.* **2016**, 3605643 (2016).
39. Cabeza-Cabrerizo, M., Cardoso, A., Minutti, C. M., Pereira da Costa, M. & Reis e Sousa, C. Dendritic cells revisited. *Annu. Rev. Immunol.* **39**, 131–166 (2021).
40. Wu, Z. et al. Development and function of chicken $XCR1^+$ conventional dendritic cells. *Front. Immunol.* **14**, 1273661 (2023).
41. Sutton, K. M. et al. Characterization of conventional dendritic cells and macrophages in the spleen using the CSF1R-reporter transgenic chickens. *Front. Immunol.* **12**, 636436 (2021).
42. Härtle, S., Sutton, K., Vervelde, L. & Dalgaard, T. S. Delineation of chicken immune markers in the era of omics and multicolor flow cytometry. *Front. Vet. Sci.* **11**, 1385400 (2024).
43. King, C. et al. TGF-beta1 alters APC preference, polarizing islet antigen responses toward a Th2 phenotype. *Immunity* **8**, 601–613 (1998).
44. Sanjabi, S., Oh, S. A. & Li, M. O. Regulation of the immune response by TGF-β: from conception to autoimmunity and infection. *Cold Spring Harb. Perspect. Biol.* **9**, a022236 (2017).
45. Gattinoni, L. et al. A human memory T cell subset with stem cell-like properties. *Nat. Med.* **17**, 1290–1297 (2011).
46. Bradley, L. M., Haynes, L. & Swain, S. L. IL-7: maintaining T-cell memory and achieving homeostasis. *Trends Immunol.* **26**, 172–176 (2005).
47. Sallusto, F., Lenig, D., Förster, R., Lipp, M. & Lanzavecchia, A. Two subsets of memory T lymphocytes with distinct homing potentials and effector functions. *Nature* **401**, 708–712 (1999).
48. Delamarre, L., Pack, M., Chang, H., Mellman, I. & Trombetta, E. S. Differential lysosomal proteolysis in antigen-presenting cells determines antigen fate. *Science* **307**, 1630–1634 (2005).
49. Liu, F. et al. The Genome Resequencing of TCR loci in Gallus gallus revealed their distinct evolutionary features in avians. *Immunohorizons* **4**, 33–46 (2020).
50. Cyster, J. G. & Allen, C. D. C. B cell responses: cell interaction dynamics and decisions. *Cell* **177**, 524–540 (2019).
51. Lee, S. W. et al. Attenuated vaccines can recombine to form virulent field viruses. *Science* **337**, 188 (2012).
52. Thomas, S., Abraham, A., Rodríguez-Mallon, A., Unajak, S. & Bannantine, J. P. Challenges in veterinary vaccine development. *Methods Mol. Biol.* **2411**, 3–34 (2022).
53. Al-Rasheed, M., Ball, C. & Ganapathy, K. Route of infectious bronchitis virus vaccination determines the type and magnitude of

immune responses in table egg laying hens. *Vet. Res.* **52**, 139 (2021).
54. Bhuiyan, M. S. A. et al. Infectious bronchitis virus (Gammacoronavirus) in poultry farming: vaccination, immune response and measures for mitigation. *Vet. Sci.* **8**, 2732021 (2021).
55. Al-Rasheed, M., Ball, C., Parthiban, S. & Ganapathy, K. Evaluation of protection and immunity induced by infectious bronchitis vaccines administered by oculonasal, spray or gel routes in commercial broiler chicks. *Vaccine* **41**, 4508–4524 (2023).
56. Lopes, P. D. et al. Inactivated infectious bronchitis virus vaccine encapsulated in chitosan nanoparticles induces mucosal immune responses and effective protection against challenge. *Vaccine* **36**, 2630–2636 (2018).
57. Li, X. et al. How to break through the bottlenecks of in ovo vaccination in poultry farming. *Vaccines* **12**, 48 (2024).
58. Dai, M. et al. Duck $CD8^+$ T cell response to H5N1 highly pathogenic avian influenza virus infection in vivo and in vitro. *J. Immunol.* **209**, 979–990 (2022).
59. Dai, M. et al. Dissection of key factors correlating with H5N1 avian influenza virus driven inflammatory lung injury of chicken identified by single-cell analysis. *PLoS Pathog.* **19**, e1011685 (2023).
60. Shah, A. U. et al. From nasal to basal: single-cell sequencing of the bursa of Fabricius highlights the IBDV infection mechanism in chickens. *Cell Biosci.* **11**, 212 (2021).
61. Qu, X., Li, X., Li, Z., Liao, M. & Dai, M. Chicken peripheral blood mononuclear cells response to avian leukosis virus subgroup J infection assessed by single-cell RNA sequencing. *Front Microbiol* **13**, 800618 (2022).
62. Warren, W. C. et al. The immune cell landscape and response of Marek's disease resistant and susceptible chickens infected with Marek's disease virus. *Sci. Rep.* **13**, 5355 (2023).
63. Reed, L. J. & Muench, H. A simple method of estimating fifty per cent endpoint. *Am. J. Hyg.* **27**, 493–497 (1938).
64. Zhang, Y., Han, Z., Li, H. & Liu, S. Development of a recombinant enzyme-linked immunosorbent assay for the detection of antibodies against infectious bronchitis virus. *Viral Immunol.* **36**, 649–658 (2023).
65. Huang da, W., Sherman, B. T. & Lempicki, R. A. Systematic and integrative analysis of large gene lists using DAVID bioinformatics resources. *Nat. Protoc.* **4**, 44–57 (2009).
66. Stuart, T. et al. Comprehensive integration of single-cell data. *Cell* **177**, 1888–1902 (2019).
67. Becht, E. et al. Dimensionality reduction for visualizing single-cell data using UMAP. *Nat. Biotechnol.* **37**, 38–44 (2019).
68. Linderman, G. C., Rachh, M., Hoskins, J. G., Steinerberger, S. & Kluger, Y. Fast interpolation-based t-SNE for improved visualization of single-cell RNA-seq data. *Nat. Methods* **16**, 243–245 (2019).
69. Houssaint, E., Lassila, O. & Vainio, O. Bu-1 antigen expression as a marker for B cell precursors in chicken embryos. *Eur. J. Immunol.* **19**, 239–243 (1989).
70. Nera, K. P. et al. Loss of Pax5 promotes plasma cell differentiation. *Immunity* **24**, 283–293 (2006).
71. Viertlboeck, B. C. & Göbel, T. W. Chicken thrombocytes express the CD51/CD61 integrin. *Vet. Immunol. Immunopathol.* **119**, 137–141 (2007).
72. Vu Manh, T. P. et al. Existence of conventional dendritic cells in *Gallus gallus* revealed by comparative gene expression profiling. *J. Immunol.* **192**, 4510–4517 (2014).
73. You, Z. et al. Integrated analysis of lncRNA and mRNA repertoires in Marek's disease infected spleens identifies genes relevant to resistance. *BMC Genomics* **20**, 245 (2019).
74. Hao, X. L. et al. Establishing a multicolor flow cytometry to characterize cellular immune response in chickens following H7N9 avian influenza virus infection. *Viruses* **12**, 1396 (2020).
75. Wu, Z. G. et al. Development of novel reagents to chicken FLT3, XCR1 and CSF2R for the identification and characterization of avian conventional dendritic cells. *Immunology* **165**, 171–194 (2022).
76. Trapnell, C. et al. The dynamics and regulators of cell fate decisions are revealed by pseudotemporal ordering of single cells. *Nat. Biotechnol.* **32**, 381–386 (2014).
77. Jin, S. Q. et al. Inference and analysis of cell-cell communication using CellChat. *Nat. Commun.* **12**, 1088 (2021).

Acknowledgements

We are grateful to Dr. Zongxi Han, Dr. Yuzhu Hou, Dr. Zhijie Chen, Miss Yanhui Zhang, and other colleagues for providing technical support and valuable suggestions. This work was supported by the National Key R&D Program of China [grant number 2021YFD1801105], the National Natural Science Foundation of China [grant number 32072853], the Natural Science Foundation of Heilongjiang Province of China [grant number JQ2021C006], and the Agriculture Research System of China [grant number CARS-40-K18].

Author contributions

H.L., S.L., and Z.X. designed the study and wrote the manuscript with critical inputs from X.L. (Xuefeng Li), Y.L., Y.Z., and B.F.; X.L. (Xuefeng Li), B.F., and H.L. conducted all analyses with the help of M.X., S.F., X.L. (Xiaoxiao Liu), and Z.X.; X.L. (Xuefeng Li), Y.L., and Y.Z. managed and contributed to animal experiments and all related detections with help from Z.L., L.C., and L.X.; H.L., X.L. (Xuefeng Li), and Y.L. managed and contributed to sample collection of scRNA-seq data with help from L.C.; All authors contributed to the final manuscript.

Competing interests

The authors declare no competing interests.

Additional information

Supplementary information The online version contains supplementary material available at https://doi.org/10.1038/s41541-025-01154-5.

Correspondence and requests for materials should be addressed to Zhengtao Xiao, Shengwang Liu or Hai Li.